Large One-Loop Effects of BSM Triple Higgs Couplings on Double Higgs Production at e^+e^- Colliders

F. Arco[1,2*,3†], S. Heinemeyer[4‡] and M. Mühlleitner[3§]

[1] *Deutsches Elektronen-Synchrotron DESY, Notkestr. 85, 22607 Hamburg, Germany*

[2] *Institute for Astroparticle Physics, Karlsruhe Institute of Technology,*
Hermann-von-Helmholtz-Platz 1, 76344 Eggenstein-Leopoldshafen, Germany

[3] *Institute for Theoretical Physics, Karlsruhe Institute of Technology,*
Wolfgang-Gaede-Str. 1, 76131 Karlsruhe, Germany

[4]*Instituto de Física Teórica (UAM/CSIC), Universidad Autónoma de Madrid,*
Cantoblanco, 28049, Madrid, Spain

Abstract

The measurement of the Higgs boson self-coupling is crucial for our understanding of the nature of electroweak symmetry breaking and potential physics beyond the Standard Model (BSM). In this work, we study in the framework of the 2-Higgs-Doublet Model (2HDM) the impact of one-loop corrections to triple Higgs couplings (THCs) on the pair production of two Standard Model (SM)-like Higgs bosons h at future high-energy e^+e^- colliders, focusing on the $e^+e^- \to Zhh$ process. By including the one-loop corrections to the THCs relevant for this process, i.e. the coupling between three SM-like Higgs bosons, λ_{hhh}, and between the non-SM-like Higgs H, assumed to be heavier, and two SM-like Higgs bosons, λ_{hhH}, we account for the leading one-loop corrections to the di-Higgs production cross section. We show that the one-loop corrected THC λ_{hhh} can be enhanced up to nearly six times its SM value, which substantially enhances the di-Higgs production cross section w.r.t. the tree-level prediction, even in the alignment limit. On the other hand, one-loop corrections to λ_{hhH} can also enhance its value, potentially yielding to more prominent heavy Higgs H resonant production. We explore the sensitivity to the loop-corrected λ_{hhh} and the possible access to λ_{hhH} via the H resonant peak at a future high-energy e^+e^- collider, such as the ILC. We highlight the fact that including the one-loop corrected THCs can enhance the sensitivity to the H resonant peak, and therefore to λ_{hhH}. Finally, we discuss the required experimental precision at future e^+e^- colliders necessary to achieve these sensitivities.

---

* Former address.
†email: Francisco.Arco@desy.de
‡email: Sven.Heinemeyer@cern.ch
§email: Milada.Muehlleitner@kit.edu

1 Introduction

The discovery of the Higgs boson in 2012 by the ATLAS and CMS collaborations [1, 2] constituted a milestone in particle physics and structurally completed the Standard Model (SM). To date, all the measured signal strengths for the discovered Higgs boson are consistent with the SM predictions within the experimental and theoretical uncertainties [3, 4]. However, the access to the Higgs-boson self interactions at the LHC is very challenging and only upper limits could be set on the di-Higgs production cross section, which is used to measure the triple Higgs coupling (THC). In particular, the ratio of the triple Higgs self-coupling to its SM value at the tree level, denoted by κ_λ, is only constrained to be within the interval $-1.2 < \kappa_\lambda < 7.2$ at 95% C.L. as reported by ATLAS [5], and within $-1.4 < \kappa_\lambda < 7.8$ at 95% C.L. as reported by CMS [6]. Therefore, the Higgs-boson potential is so far largely unconstrained, leaving plenty of room for new physics in the Higgs sector. Consequently, there have been many phenomenological studies of possible new scalar sectors from extended beyond the SM (BSM) Higgs sectors. Such models predict the existence of new Higgs bosons and new scalar interactions among them. A well studied extension of the SM Higgs-boson sector is the 2-Higgs-Doublet Model (2HDM) [7–10], which consists of adding a second complex Higgs doublet to the SM Higgs sector implying the existence of five physical Higgs bosons: two charged Higgs bosons $H^\pm$, two neutral $\mathcal{CP}$-even Higgs bosons h and H (with $m_h < m_H$), and one neutral $\mathcal{CP}$-odd scalar A. In this work, the Higgs boson h is identified with the discovered Higgs boson at the LHC, and the remaining Higgs bosons are assumed to be heavier. The Higgs boson h will be referred to as SM-like Higgs boson in the following.

In particular, the THC of the SM-like Higgs-boson, λ_{hhh}, in the context of the 2HDM has been studied extensively. At tree level, this coupling can only present deviations of at most -100% and +20% w.r.t. its SM prediction in specific regions of the parameter space allowed by all theoretical and experimental constraints [11–14]. On the contrary, the couplings of the SM-like Higgs boson to two other heavier Higgs bosons can be large, even in the alignment limit. In particular, in the 2HDM large mass differences between the heavy Higgs bosons can induce large triple and quartic scalar couplings between Higgs bosons, which are only constrained by the requirement of unitarity [12, 14]. In turn, such large values of the scalar couplings can induce large loop corrections to the Higgs boson self-coupling in extended Higgs sectors. These higher-order corrections are known and have been studied at the one-loop level [15–17], and even the two-loop level [18–20] in the context of the 2HDM. Although higher-order corrections to other scalar couplings have been less studied in the literature, they could potentially exhibit similar higher-order effects as λ_{hhh}, since a comparable set of scalar couplings enters in their predictions. Other extended Higgs sectors are expected to exhibit large higher-order corrections in the case that large scalar couplings can be realized (see for instance [17, 21–24] and references therein). The higher-order corrections to the Higgs potential can have significant phenomenological consequences. As an example, they are crucial to study the thermal cosmological evolution of BSM models in the search for a possible first-order electroweak phase transition (FOEWPT). For instance, it was found in Refs. [25, 26] that the region of the parameter space in the 2HDM that leads to a FOEWPT requires values of κ_λ around 2, which can only be realized at the loop level.

In the investigation of the Higgs sector, not only hadron colliders, such as the LHC and the HL-LHC will be relevant, but also future e^+e^- colliders will play a crucial role [27, 28].

In particular, at energies below about $\sqrt{s} = 1$ TeV the most relevant process is the double Higgs-strahlung process, $e^+e^- \to Zhh$. At energies above ~ 1 TeV W boson fusion into Higgs pairs, $e^+e^- \to \nu\nu hh$, is the main production channel [29–35]. There are several proposals for high-energy e^+e^- colliders, for example, the International Linear Collider (ILC) [36], the Compact Linear Collider (CLIC) [34], the Cool Cooper Collider (C^3) [37] or the Linear Collider Facility (LCF) at CERN [38, 39]. Overall, these proposed high-energy linear colliders could reach a 10-20% accuracy in the measurement of κ_λ, for the case $\kappa_\lambda = 1$, see for instance Refs. [40–42]. The sensitivity projections for the measurement of a non-SM-like triple Higgs coupling where $\kappa_\lambda \neq 1$ can be found in Refs. [39, 43, 44].[1] It should be noted that other planned e^+e^- circular colliders, such as the Future Circular Collider (FCC-ee) [46] or the Circular Electron Positron Collider (CEPC) [47, 48], have only limited access to λ_{hhh}, since it can only be accessed indirectly via higher-order loop corrections to the single Higgs production cross section (see for instance Refs. [27, 28]). Consequently, we focus on high-energy linear e^+e^- colliders in this work.

In this paper, we study the impact of the one-loop corrections to the THCs. In a first step we determine the intervals of λ_{hhh} and λ_{hhH}, evaluated at the one-loop level, that are allowed by all relevant experimental and theoretical constraints (updating the corresponding analyses in Refs. [12–14]). The main part of our work analyzes the impact of the loop-corrected THCs on double Higgs production in the channel $e^+e^- \to Zhh$. We assume the foreseen ILC operating stages at the center-of-mass energies of 500 GeV and 1 TeV, with their anticipated integrated luminosity and polarization of the electron and positron beams [36, 49]. The production of two Higgs bosons at e^+e^- colliders at tree-level and the potential access to THCs in the 2HDM (and the MSSM) has been studied before in Refs. [29–32, 35, 50–55]. Our computation uses the analytic tree-level formulas from Refs. [31, 32] for the di-Higgs production cross section, adapted to the 2HDM, with the inclusion of the THCs λ_{hhh} and λ_{hhH} evaluated at the one loop level. We employ the Coleman-Weinberg effective potential approach [56, 57] to obtain the one-loop corrections to the THCs. In particular, we use the results obtained from the implementation of the 2HDM effective potential in the public code `BSMPT` [58–60]. Moreover, in the case of λ_{hhh}, we also perform a diagrammatic one-loop computation using the public code `anyH3/anyBSM` [17]. With this full-diagrammatic approach, we can evaluate the effect of the finite-momentum dependence of the one-loop corrected λ_{hhh} entering the cross section prediction, which is neglected in the effective potential computation. The inclusion of the couplings λ_{hhh} and λ_{hhH} at the one-loop level, denoted as $\lambda_{hhh}^{(1)}$ and $\lambda_{hhH}^{(1)}$, respectively, in the calculation of $e^+e^- \to Zhh$ takes into account the main one-loop electroweak (EW) corrections. We demonstrate in this work that they can significantly enhance the production cross section by up to a factor of five w.r.t. the tree-level prediction. In the context of the (HL-)LHC the effect of BSM one-loop corrected $\lambda_{hhh}^{(1)}$ and $\lambda_{hhH}^{(1)}$ on di-Higgs production has been considered in [61, 62].

To study the sensitivity to the one-loop corrected THCs, we analyze the differential cross section as a function of the di-Higgs invariant mass m_{hh}. Here we take into account the main decay channel into four b-quarks, as well as detector cuts and b-tagging efficiencies. We find that the large one-loop corrections to λ_{hhh} can strongly enhance the non-resonant contributions

---

[1]Recently, the ATLAS and CMS collaborations published the projection on the precision of the determination of κ_λ at the HL-LHC for the case $\kappa_\lambda \neq 1$ [45].

to the di-Higgs production cross section, even in the alignment limit. Furthermore, the obtained m_{hh} distributions exhibit, as expected, a clear peak-dip (or dip-peak) structure around $m_{hh} = m_H$, which may yield access to λ_{hhH}. In this context, several experimental uncertainties have to be considered. The experimental uncertainty in the m_{hh} measurement is taken into account by a Gaussian smearing of our theoretical cross section distributions. On top of that a finite resolution in m_{hh} (i.e. a binning in m_{hh}) has to be considered. We quantify the possible sensitivity to the H resonant peak, and thus to λ_{hhH}, by means of the significance of the H resonant peak against the no-resonance hypothesis as given by a likelihood profile ratio [63]. Our results indicate that indeed a high-energy e^+e^- collider may give access to the BSM THC λ_{hhH}.

The paper is organized as follows: In Sect. 2 we introduce the 2HDM and its scalar couplings, fix our notation, and we discuss how we compute the THCs λ_{hhh} and λ_{hhH} at the one-loop level. In Sect. 3 we give the currently allowed ranges for the tree-level and one-loop corrected THCs λ_{hhh} and λ_{hhH}, taking into account all relevant theoretical and current experimental constraints. In Sect. 4 we describe how we compute the di-Higgs cross section in the 2HDM and discuss possible sources of experimental uncertainty, such as detector acceptance, reconstruction efficiency, detector resolution, and cross section binning. In Sect. 5 we analyze the differential distributions of the double Higgs production cross section including one-loop THCs and analyze the potential experimental sensitivity to them. Finally, in Sect. 6 we present our conclusions.

2   The 2HDM and its Scalar Couplings

The 2HDM [8–10] adds a second complex Higgs doublet to the SM Higgs sector. The renormalizable scalar potential for the two $SU(2)_L$ Higgs doublets, Φ_1 and Φ_2, reads

$$
V_{\text{2HDM}}^{(0)} = m_{11}^2 \left(\Phi_1^\dagger \Phi_1 \right) + m_{22}^2 \left(\Phi_2^\dagger \Phi_2 \right) - \left[m_{12}^2 \left(\Phi_1^\dagger \Phi_2 \right) + \text{h.c.} \right] + \frac{\lambda_1}{2} \left(\Phi_1^\dagger \Phi_1 \right)^2 +
$$
$$
\frac{\lambda_2}{2} \left(\Phi_2^\dagger \Phi_2 \right)^2 + \lambda_3 \left(\Phi_1^\dagger \Phi_1 \right) \left(\Phi_2^\dagger \Phi_2 \right) + \lambda_4 \left(\Phi_1^\dagger \Phi_2 \right) \left(\Phi_2^\dagger \Phi_1 \right) + \left[\frac{\lambda_5}{2} \left(\Phi_1^\dagger \Phi_2 \right)^2 + \text{h.c.} \right] .
$$

(1)

We assume $\mathcal{CP}$ conservation in the Higgs sector so that all mass and coupling parameters in the potential are real. Furthermore, the potential in Eq. (1) respects a Z_2 symmetry (with $\Phi_1 \to \Phi_1$ and $\Phi_2 \to -\Phi_2$), which is imposed to avoid flavor-changing neutral currents at tree-level [64, 65].

The 2HDM predicts five physical Higgs bosons, two $\mathcal{CP}$-even Higgs bosons, h and H (with $m_h < m_H$), one $\mathcal{CP}$-odd Higgs boson, A, and a pair of charged Higgs bosons, $H^\pm$. The angle α diagonalizes the $\mathcal{CP}$-even sector of the model, while the angle β diagonalizes the $\mathcal{CP}$-odd and the charged sectors, with $\tan\beta$ given by the ratio of the two vacuum expectation values (vevs) of the two Higgs doublets, $\tan\beta = v_2/v_1$. The vevs satisfy the relation $v_1^2 + v_2^2 = v^2$, where $v = \left(\sqrt{2}\, G_F \right)^{-1/2} \simeq 246.22$ GeV is the SM vev.

The 2HDM Higgs couplings to the SM particles are modified w.r.t. to the corresponding SM Higgs couplings. The modification factors for the h, H, A couplings to the massive massive gauge bosons $V = Z, W$ are given by

$$
\xi_V^h = s_{\beta-\alpha}, \quad \xi_V^H = c_{\beta-\alpha}, \quad \xi_V^A = 0,
$$

(2)

	Type I	Type II	Type III, Y or Flipped (FL)	Type IV, X or Lepton-Specific (LS)
ξ_u	$\cot\beta$	$\cot\beta$	$\cot\beta$	$\cot\beta$
ξ_d	$\cot\beta$	$-\tan\beta$	$-\tan\beta$	$\cot\beta$
ξ_l	$\cot\beta$	$-\tan\beta$	$\cot\beta$	$-\tan\beta$

Table 1: Values for ξ_f in the four Z_2 conserving 2HDM Yukawa types.

where we have introduced the short-hand notation $s_x = \sin x$ and $c_x = \cos x$. Due to the assumed $\mathcal{CP}$ conservation, the pseudoscalar does not couple to the massive gauge bosons. In the Yukawa sector, the imposed Z_2 symmetry leads to four distinct Yukawa sectors. The values of the Higgs coupling modification factors $\xi_f^{h,H,A}$ to the fermions (modulo a factor γ_5 in the pseudoscalar couplings to the fermions) can be expressed as

$$\xi_f^h = s_{\beta-\alpha} + \xi_f c_{\beta-\alpha} \,, \quad \xi_f^H = c_{\beta-\alpha} - \xi_f s_{\beta-\alpha} \,, \quad \xi_u^A = -i\xi_u \,, \quad \xi_{d,l}^A = i\xi_{d,l} \,. \tag{3}$$

The corresponding ξ_f ($f = u, d, l$) for the up-type, down-type and lepton couplings, respectively, in the four 2HDM Yukawa types are given in Tab. 1.

As it can be inferred from Eqs. (2) and (3), in the limit $c_{\beta-\alpha} \to 0$ the light $\mathcal{CP}$-even Higgs boson has the same couplings (at tree-level) to the SM particle content as predicted by the SM [66]. Therefore, by keeping $c_{\beta-\alpha}$ close to zero, one can get a h Higgs boson with similar properties as the SM one. However, one should keep in mind that there are still non-SM couplings that do not vanish in this so-called *alignment limit*, such as ZHA or γH^+H^-, and even couplings involving the h Higgs boson, such as hHH, hAA or hH^+H^-.

The potential in Eq. (1) introduces eight free parameters in the model. The minimization conditions allow to relate the parameters m_{11}^2 and m_{22}^2 with $\tan\beta$ and v. The masses of the physical Higgs bosons can be related to the remaining parameters of the potential, the mixing angles α and β, and the soft-breaking parameter m_{12}^2 (see e.g. Ref. [12] for the explicit expressions). Therefore, the input parameters of the 2HDM can be given in the so-called "physical" basis

$$v \,, \quad m_h \,, \quad m_H \,, \quad m_A \,, \quad m_{H^\pm} \,, \quad \tan\beta \,, \quad c_{\beta-\alpha} \,, \quad m_{12}^2 \,. \tag{4}$$

For later convenience, we define the parameter $\bar{m}^2$, which is related to the soft-breaking parameter m_{12}^2 as

$$\bar{m}^2 = \frac{m_{12}^2}{\sin\beta\cos\beta} \,. \tag{5}$$

In this paper, we always identify the light $\mathcal{CP}$-even Higgs boson with the Higgs boson discovered at the LHC, and therefore we set $m_h = 125.25$ GeV [67]. This, together with the fact that v is also fixed, leads to a total of six free parameters in our analysis.

2.1 Tree-Level Scalar Higgs Couplings

The potential from Eq. (1) leads to new triple scalar interactions among the physical Higgs bosons that we denote generically as:

$$\mathcal{L}_{\text{scalar}} \supset -v \sum_{i,j,k} \lambda^{(0)}_{h_i h_j h_k} h_i h_j h_k \,, \tag{6}$$

where $h_{i,j,k}$ refers to the five physical Higgs bosons present in the 2HDM. We will refer to the parameter $\lambda^{(0)}_{h_i h_j h_k}$ as the tree-level triple Higgs coupling (THC) between the Higgs bosons h_i, h_j and h_k. We adopt this convention to resemble the SM Higgs self-interaction, where $\mathcal{L}_{\text{scalar}}^{\text{SM}} \supset -v\lambda_{\text{SM}}^{(0)} h_{\text{SM}}^3$ with h_{SM} being the SM Higgs boson and

$$\lambda_{\text{SM}}^{(0)} = \frac{m_{h_{\text{SM}}}^2}{2v^2} \simeq 0.13 \,, \tag{7}$$

where we assume $m_h = m_{h_{\text{SM}}}$ in this work. The Feynman rule for the interaction between three Higgs bosons in terms of this THC then reads

$$h_i h_j h_k : \qquad -ivn! \, \lambda^{(0)}_{h_i h_j h_k} \,, \tag{8}$$

where n is the number of identical particles in the vertex.

   We provide the 2HDM tree-level predictions for the couplings $\lambda^{(0)}_{hhh}$ and $\lambda^{(0)}_{hhH}$ since they enter the $e^+ e^- \to Zhh$ cross section,

$$\lambda^{(0)}_{hhh} = \frac{1}{2v^2} \left(s_{\beta-\alpha}^3 m_h^2 + s_{\beta-\alpha} c_{\beta-\alpha}^2 \left(3m_h^2 - 2\bar{m}^2 \right) + 2c_{\beta-\alpha}^3 \cot 2\beta \left(m_h^2 - \bar{m}^2 \right) \right) , \tag{9}$$

$$\begin{aligned} \lambda^{(0)}_{hhH} = \frac{-c_{\beta-\alpha}}{2v^2} \Big(& s_{\beta-\alpha}^2 \left(2m_h^2 + m_H^2 - 4\bar{m}^2 \right) + 2s_{\beta-\alpha} c_{\beta-\alpha} \cot 2\beta \left(2m_h^2 + m_H^2 - 3\bar{m}^2 \right) \\ & - c_{\beta-\alpha}^2 \left(2m_h^2 + m_H^2 - 2\bar{m}^2 \right) \Big) \,. \end{aligned} \tag{10}$$

It should be noted that in the alignment limit, one finds $\lambda^{(0)}_{hhh} = \lambda_{\text{SM}}^{(0)}$ and $\lambda^{(0)}_{hhH} = 0$. This can change, however, when one-loop corrections to these couplings are considered, as will be discussed in the following sections.

   In our evaluation of the one-loop corrected THCs, denoted by $\lambda^{(1)}_{hhh}$ and $\lambda^{(1)}_{hhH}$ in the following, all tree-level triple and quartic scalar couplings involving the h and H bosons can play a relevant role in the prediction. Therefore, for reference, we provide the Feynman rules of such interactions in the alignment limit (i.e. $c_{\beta-\alpha} = 0$),

$$hhh/v = hhhh : \qquad \frac{-3im_h^2}{v^2} = -6i\lambda_{\text{SM}}^{(0)} \,, \tag{11}$$

$$hhH = hhhH : \qquad 0 \,, \tag{12}$$

$$hHH/v = hhHH : \qquad \frac{-i\left(m_h^2 + 2m_H^2 - 2\bar{m}^2\right)}{v^2} \,, \tag{13}$$

$$h\phi\phi/v = hh\phi\phi : \qquad \frac{-i\left(m_h^2 + 2m_\phi^2 - 2\bar{m}^2\right)}{v^2} \,, \tag{14}$$

$$HHH/(3v) = hHHH/3 = H\phi\phi/v = hH\phi\phi : \qquad \frac{2i\left(m_H^2 - \bar{m}^2\right)\cot 2\beta}{v^2} \,, \tag{15}$$

where ϕ refers to A or $H^\pm$. For a complete set of Feynman rules for triple and quartic Higgs couplings in the $\mathcal{CP}$-conserving 2HDM outside the alignment limit, see App. A of Ref. [68].

2.2 One-Loop Triple Higgs Couplings

The one-loop corrected triple Higgs couplings in the 2HDM can be obtained in the limit of vanishing external momenta from the effective potential, or alternatively, in the diagrammatic approach which includes the finite momentum effects. We use the loop-corrected couplings obtained in both approaches.

In order to get the loop-corrected THCs in the effective potential approach we use the public code BSMPTv3 [58–60], where the trilinear Higgs self-couplings are calculated from the third derivatives of the one-loop corrected effective potential with respect to the corresponding scalar fields. In BSMPT, the $\overline{\text{MS}}$-renormalized effective potential at the renormalization scale $\mu = v \approx 246.22$ GeV receives additional finite counterterms, which in an on-shell-like renormalization scheme fix the mixing matrix elements in the Higgs mass matrices to their tree-level values, such that the masses and Higgs coupling modification factors are renormalized to their leading-order values. The trilinear Higgs self-couplings, however, obtain non-zero loop corrections. For details, we refer the reader to Ref. [58].

The computation of the loop-corrected THCs in the diagrammatic approach is done with the code anyH3/anyBSM [17], which evaluates in a semi-automatic way the THC of the SM-like Higgs boson in a plethora of BSM models with extended Higgs sectors, including the 2HDM. The result is obtained in the 't Hooft-Feynman gauge. The masses are renormalized on-shell, and for the mixing angles α and β the scheme described in [16] is applied. The parameter m_{12}^2 is renormalized in the $\overline{\text{MS}}$ scheme. The VEV counterterm is derived from the counterterms of m_W, m_Z and the electric charge e, applying its on-shell relation to these quantities. The electric charge is renormalized on-shell in the Thomson limit. For details, we refer to Ref. [17].

We will use the definition $\kappa_\lambda^{(1)}$ as the value of the one-loop corrected coupling $\lambda_{hhh}^{(1)}$ with respect to the SM tree-level value $\lambda_{\text{SM}}^{(0)}$,

$$\kappa_\lambda^{(1)} = \frac{\lambda_{hhh}^{(1)}}{\lambda_{\text{SM}}^{(0)}}, \tag{16}$$

which corresponds to the variable used in the experimental analyses.

Due to the simplicity of the formulae, we give some sample results here in the effective potential approach. In the SM, the main one-loop correction to the h_{SM} triple self-coupling is the top-mediated loop diagram, which leads to [15]

$$\lambda_{\text{SM}}^{(1)} = \lambda_{\text{SM}}^{(0)} \left(1 - \frac{m_t^4}{\pi^2 m_{h_{\text{SM}}}^2 v^2} \right). \tag{17}$$

This implies a correction of about -9% for $\kappa_\lambda^{(1)}$ in the SM. In addition to this, in the 2HDM this coupling can receive new loop-corrections from the new scalar interactions between three and four Higgs bosons. The main contributions in the alignment limit can be written as [15]

$$\lambda_{hhh}^{(1)} \simeq \lambda_{\text{SM}}^{(0)} \left(1 - \frac{m_t^4}{\pi^2 m_h^2 v^2} + \sum_{\phi = H, A, H^\pm} \frac{n_\phi m_\phi^4}{12\pi^2 m_h^2 v^2} \left(1 - \frac{\bar{m}^2}{m_\phi^2} \right)^3 \right), \tag{18}$$

with $n_H = n_A = 1$ and $n_{H^\pm} = 2$. The first term is the top loop contribution, as in the SM, but the remaining terms are pure Higgs contributions. In particular, in the limit where $m_H, m_A, m_{H^\pm} \gg \bar{m}$, corresponding to large scalar couplings (see Sect. 2.1), these purely scalar corrections can become very large and be well above the size of the top-quark contributions.

3 Currently Allowed Values for the THCs λ_{hhh} and λ_{hhH}

In this section, we explore how large the one-loop corrections to the THCs λ_{hhh} and λ_{hhH} can be in the 2HDM while respecting all relevant theoretical and experimental constraints of the model. Moreover, we discuss in which regions of the parameter space we find large one-loop corrections, and which class of loop corrections are responsible for them. Concerning the higher-order corrections, in this section, we concentrate on the results for the one-loop THCs obtained in the effective potential approach (as described in Sect. 2.2).

3.1 Theoretical and Experimental Constraints

To evaluate the currently allowed ranges for the THCs λ_{hhh} and λ_{hhH} (at tree-level and at one-loop), we performed a scan of the 2HDM parameter space by using the public code `ScannerS` [69, 70]. In the following, we summarize the main constraints on the 2HDM and how they are applied by `ScannerS`:

- **Electroweak precision data:** The oblique parameters S, T and U are a common way to parametrize BSM radiative corrections to the EW gauge boson self-energies. We use the 2σ allowed region given by the reported values by the PDG23 fit [67]: $S = -0.02 \pm 0.10$, $T = 0.03 \pm 0.12$ and $U = 0.01 \pm 0.11$, with correlations $\rho_{ST} = 0.92$, $\rho_{SU} = -0.80$ and $\rho_{TU} = -0.93$. The most constraining parameter is T, which can receive large corrections in the 2HDM. To keep these corrections small, the mass of one of the neutral Higgs bosons, m_H and/or m_A, should be close to the mass of the charged Higgs boson, i.e. $m_H \sim m_{H^\pm}$ and/or $m_A \sim m_{H^\pm}$ [71].

- **Tree-level perturbative unitarity:** We require that the eigenvalues of the $2 \to 2$ scalar scattering matrix for the lowest term in the partial wave expansion are below the unitarity limit in the large energy limit. This leads to the condition $|\text{Re}(a_0)| < 1/2$ (see Refs. [72, 73] for the explicit expressions for a_0).

- **Potential stability:** We impose the bounded-from-below condition to the potential, i.e. we require that it does not go to minus infinity in any direction in the Φ_1–Φ_2 plane [74]. In addition, we also require that the EW minimum is a global minimum of the potential [75]. We do not consider the possibility that the EW minimum is meta-stable with a tunneling time larger than the age of the universe, which could enlarge the allowed region of the model.

- **BSM Higgs boson searches:** We consider all current searches for BSM Higgs bosons at the LHC, Tevatron and LEP, which typically impose bounds on the production cross

sections times branching ratio of these new states at the 95% confidence level (CL). For each point in the parameter space, we identify the most sensitive channel according to the expected experimental bound and then check whether or not it is excluded by the experimental result. We impose these bounds with the help of the public code `HiggsBounds` [76–80], as part of `HiggsTools` [81].

- **Signal strength measurements for the SM-like Higgs boson:** We require statistical compatibility between the signal strength measurements for the discovered Higgs boson to date, and the model predictions for the light $\mathcal{CP}$-even Higgs boson h. We perform a χ^2 statistical analysis between the 2HDM predicted and experimentally measured signal strengths of the SM-like Higgs boson, and for simplicity we require compatibility with the SM prediction at the 2σ level (i.e. $\Delta\chi^2 \leq 6.18$ in the case of a two-dimensional plane), where the result of the SM fit is $\chi^2_{\mathrm{SM}} = 152.54$ with 159 observables. For this we use the code `HiggsSignals` [82–84], as a part of `HiggsTools` [81].

  The 2HDM predictions for the branching ratios of the 2HDM Higgs bosons required by `HiggsTools` as input are obtained with the public code `HDECAY6.60` [85, 86], including the state-of-the-art higher-order QCD corrections and off-shell decays. The production cross sections are computed internally in `HiggsSignals`, respectively, `HiggsTools`, applying the appropriate coupling rescaling factors.

- **Flavor Observables:** Flavor-changing neutral-current processes can receive additional contributions in the 2DHM from the charged Higgs bosons in the loops. To take them into account we use the results of Ref. [87] at the 2σ level in the $m_{H^\pm}$–$\tan\beta$ plane.

3.2 Allowed Ranges for λ_{hhh} and λ_{hhH}

In this section we present and discuss the allowed ranges for the THCs λ_{hhh} and λ_{hhH} at tree level and at one-loop level. We generated 400,000 points allowed by the previously discussed constraints, where the input parameters of the 2HDM were varied randomly inside the following ranges,

$$m_H \in [125.25, 1500]\ \mathrm{GeV}\,, \quad m_A \in [10, 1500]\ \mathrm{GeV}\,, \quad m_{H^\pm} \in [m_{\min}, 1500]\ \mathrm{GeV}\,,$$
$$\tan\beta \in [0.1, 30]\,, \quad c_{\beta-\alpha} \in [-c_{\lim}, c_{\lim}]\,, \quad m_{12}^2 \in [0, 4\times 10^6]\ \mathrm{GeV}\,. \tag{19}$$

The value of $m_{\min}$ is set to 590 GeV for types II and FL to apply the constraint of $m_{H^\pm} \gtrsim$ 600 GeV from the flavor-changing decay $b \to s\gamma$ [87–91]. For types I and LS, we set $m_{\min} = 10$ GeV (even though these low values for the mass of the charged Higgs boson are strongly disfavored by direct searches). We set $c_{\lim} = 0.35$ for type I, since in this type larger deviations from the alignment limits are experimentally allowed, while we set $c_{\lim} = 0.2$ in type LS and $c_{\lim} = 0.1$ for the remaining types II and FL. We also performed a dedicated scan where we generated additional 150,000 points with $c_{\beta-\alpha} = 0$ to fully explore the alignment limit. This increases the number of total points in our scan to 550,000 for each 2HDM type.

The allowed ranges for κ_λ and λ_{hhH} obtained from the scan taking into account the previously described constraints, are shown in Tab. 2. We also show the allowed ranges for the difference between the one-loop and the tree-level predictions, namely

$$\Delta^{(1)}\kappa_\lambda = \kappa_\lambda^{(1)} - \kappa_\lambda^{(0)} \quad \text{and} \quad \Delta^{(1)}\lambda_{hhH} = \lambda_{hhH}^{(1)} - \lambda_{hhH}^{(0)}\,, \tag{20}$$

Type	$\kappa_\lambda^{(0)}$	$\kappa_\lambda^{(1)}$	$\Delta^{(1)}\kappa_\lambda$	$\lambda_{hhH}^{(0)}$	$\lambda_{hhH}^{(1)}$	$\Delta^{(1)}\lambda_{hhH}$
I	[-0.2, 1.2]	[0.2, 6.8]	[-0.3, 5.8]	[-1.6, 1.5]	[-2.1, 1.9]	[-1.0, 1.1]
II	[0.6, 1.0]	[0.7, 5.8]	[-0.1, 4.7]	[-1.5, 1.6]	[-1.7, 2.0]	[-0.4, 0.6]
LS	[0.5, 1.0]	[0.6, 6.3]	[-0.1, 5.3]	[-1.7, 1.7]	[-2.2, 2.1]	[-0.6, 0.7]
FL	[0.7, 1.0]	[0.8, 5.8]	[-0.1, 4.8]	[-1.6, 1.3]	[-1.9, 1.5]	[-0.5, 0.4]

Table 2: Allowed ranges for κ_λ and λ_{hhH} at tree level and at one-loop level and the differences between their respective loop-corrected and tree-level values as defined in the text, for the four 2HDM types.

to quantify the size of the one-loop corrections.

The obtained allowed ranges for the tree-level couplings $\lambda_{hhh}^{(0)}$ and $\lambda_{hhH}^{(0)}$ are compatible with the results published in Refs. [12–14], with subtle differences due to the slight changes in the constraints applied in each work. These results were extensively discussed in those works, but we briefly review them here for completeness. Type I is the only type that allows negative values for $\kappa_\lambda^{(0)}$ down to -0.2, along with values above 1, up to 1.2. This is because in type I, relatively large values of $c_{\beta-\alpha}$ and small masses are still allowed for the non-SM-like Higgs boson. In the other types, the allowed range for $\kappa_\lambda^{(0)}$ is between ~ 0.5 and exactly 1.0 (corresponding to the alignment limit). For $\lambda_{hhH}^{(0)}$, values between $\sim \pm 1.5$ are allowed in all types. These minimal and maximal values are obtained for Higgs boson masses above 1.2 TeV, $c_{\beta-\alpha} \sim \pm 0.05$ and values of $\tan\beta \sim 1$.

The allowed values for κ_λ change in a relevant way due to the one-loop corrections to κ_λ. It can be seen that very large values for $\kappa_\lambda^{(1)}$, up to ~ 5.8, can be realized in all types. These large corrections are found close to the alignment limit for $m_H \sim \bar{m} \ll m_A \sim m_{H^\pm}$, which leads to large triple and quartic couplings between the SM-like Higgs boson h and the heavy Higgs bosons A and $H^\pm$ (see Eqs. (13) to (15)). In type I and LS, even larger values of up to ~ 6.5 are also allowed for $\kappa_\lambda^{(1)}$, since in these types even lower values of m_H are still allowed, around 200 GeV. This in turn leads to large values for the relevant scalar couplings for smaller values of m_A and $m_{H^\pm}$. On the other hand, no negative values of $\kappa_\lambda^{(1)}$ are found, as the one-loop corrections are in general positive. In principle, negative one-loop contributions to κ_λ are possible, but they are found to be small. The reason is that negative values of the relevant scalar couplings for the one-loop corrections to κ_λ in the $\mathcal{CP}$-conserving 2HDM usually lead to an unstable potential, and the THCs appear in the third power. Therefore, only positive sizable corrections can be realized for $\kappa_\lambda^{(1)}$.

Let us highlight that values of $c_{\beta-\alpha}$ far from the alignment limit do not imply larger one-loop corrections to κ_λ, since the maximum values allowed for the relevant triple and quartic Higgs couplings depend only mildly on this parameter. Thus, the 2HDM can predict a very SM-like boson h in all the couplings to fermions and the EW gauge bosons, while yielding a value for $\kappa_\lambda^{(1)}$ much larger than 1 [15, 16].

Finally, we discuss the one-loop predictions for λ_{hhH}. We find the maximum and minimum allowed values of $\lambda_{hhH}^{(1)}$ for very heavy nearly degenerate Higgs boson masses (close to our scan limit) and slightly away from the alignment limit, with values of $c_{\beta-\alpha} \sim \pm 0.03$. The value of $\bar{m}$ is close to the values of the heavy Higgs boson masses, but a small splitting between

$\bar{m}$ and m_H helps to enhance the size of the one-loop corrections. The reason is that in the alignment limit the relevant couplings of H to other Higgs bosons depend on $m_H^2 - \bar{m}^2$. Since these contributions are found close to the alignment limit, these large corrections can be realized in all four 2HDM types. These large values of $\lambda_{hhH}^{(1)}$ are also a consequence of large tree-level values $\lambda_{hhH}^{(0)}$. In other words, a large value of $\lambda_{hhH}^{(1)}$ does not have to coincide with a large value of $\Delta^{(1)}\lambda_{hhH}$. For example, in type I, the relative one-loop corrections $\Delta^{(1)}\lambda_{hhH}$ can reach values between ± 1. This happens at low values for $m_H \sim m_{H^\pm} \sim \bar{m} < 200$ GeV and large and negative values of $c_{\beta-\alpha}$. In the other types, $\Delta^{(1)}\lambda_{hhH}$ only ranges between approximately ± 0.5, where the limits are found to be slightly away from the alignment limit, but with lighter nearly degenerate heavy Higgs bosons with masses around 1 TeV. It is worth mentioning that the largest one-loop corrections to $\lambda_{hhH}^{(1)}$ occur in a different region of the 2HDM parameter space compared to the one-loop corrections to $\kappa_\lambda^{(1)}$. This is due to the fact that the set of (scalar) couplings producing the largest corrections is different. For $\kappa_\lambda^{(1)}$ the important couplings are $h\phi\phi$ and $hh\phi\phi$, with $\phi = A$ or $H^\pm$, which can be large for $m_H \sim \bar{m} < m_A \sim m_{H^\pm}$, while the computation of the correction $\lambda_{hhH}^{(1)}$ always contains a coupling to H, like hhH, HHH or $hH\phi\phi$, which are small if $m_H \sim \bar{m}$.

It should be noticed that, even though the relative one-loop corrections $\Delta^{(1)}\lambda_{hhH}$ seem smaller than $\Delta^{(1)}\kappa_\lambda$, this is an artifact of the definition of $\kappa_\lambda^{(1)}$ vs. $\lambda_{hhH}^{(1)}$. While the corrections to λ_{hhh} are usually larger than to λ_{hhH}, the shift between the tree-level and one-loop predictions for λ_{hhh} and λ_{hhH} are comparable in many cases. For instance, one can compare the allowed maximum and minimum values for $\Delta^{(1)}\lambda_{hhh}$ and $\Delta^{(1)}\lambda_{hhH}$. By looking at the allowed ranges for $\Delta^{(1)}\lambda_{hhh}$ (which would mean to multiply $\Delta^{(1)}\kappa_\lambda$ by $\lambda_{SM}^{(0)} \simeq 0.13$), one can see that they are between ~ 0 and ~ 0.7, which is comparable to the maximum allowed relative one-loop corrections $\Delta^{(1)}\lambda_{hhH}$.

4 Di-Higgs Production with One-Loop Corrected THCs

4.1 Cross Section Calculation

The main focus of this paper is the analysis of THCs via the production of two SM-like Higgs bosons at e^+e^- colliders. For ILC energies, i.e. $\sqrt{s} \leq 1000$ GeV, the main di-Higgs production channel is double Higgs-strahlung $e^+e^- \to Zhh$. This process is key to the future measurement of the THC of the SM-like Higgs boson, since this coupling enters at the tree level in the cross section prediction [40]. In the 2HDM, the scalar coupling λ_{hhH} also enters in the cross section prediction at the tree level, with a possible resonant intermediate heavy Higgs boson H. The Feynman diagrams contributing to the process are depicted in Fig. 1.[2] The calculation also includes the diagrams with the identical final state Higgs bosons h exchanged in the second and third diagrams. As sketched in the last diagram with a blob, we introduce the one-loop corrected THCs $\lambda_{hhh}^{(1)}$ and $\lambda_{hhH}^{(1)}$, computed with the methods described in Sect. 2.2.

The inclusion of $\lambda_{hhh}^{(1)}$ and $\lambda_{hhH}^{(1)}$ in the cross section prediction includes the full subset of the one-loop purely scalar corrections. They are expected to be the most relevant ones in the 2HDM (or in other BSM models with extended Higgs sectors), because in general scalar

---

[2]These diagrams were plotted with `tikz-feynman` [92].

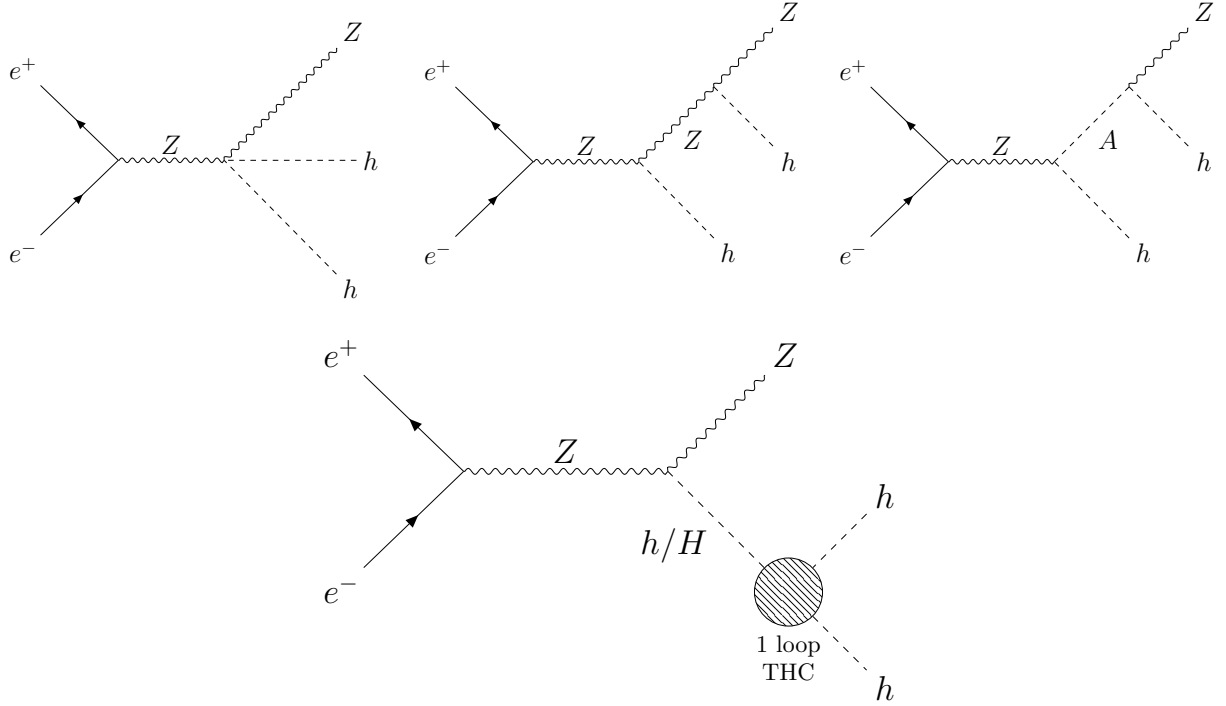**Figure 1:** Feynman diagrams contributing to the $e^+e^- \to Zhh$ cross section in the 2HDM. The blob represents the one-loop corrected triple Higgs couplings $\kappa_\lambda^{(1)}$ and $\lambda_{hhH}^{(1)}$ for the h and H-mediated diagrams, respectively.

couplings in the 2HDM can be much larger than the EW gauge coupling g. Other one-loop corrections to the cross section with potentially large scalar couplings are expected to be subleading in comparison, since they would have at least a factor of g coming from a coupling between Higgs bosons and the Z boson.

As in the SM, the diagram with κ_λ (the bottom one in Fig. 1 mediated by h) has a constructive interference with the rest of the SM-like contributions (see for example Refs. [43, 93]). Therefore, it is expected that the allowed deviations of $\kappa_\lambda^{(1)} > 1$ that can be realized in the 2HDM at the one-loop level (see Sect. 3) lead to an increase of the double Higgs-strahlung cross section. Consequently, this would imply a higher accuracy in the experimental measurement of the cross section and also of the SM-like Higgs self-coupling, as discussed in Refs. [40, 43, 44].

For our calculation we use the analytic formulas for the unpolarized differential cross section from Refs. [31, 32]. They were derived in the MSSM, and we adapted them to the 2HDM case. The differential cross section is given in terms of the reduced energies of the Higgs bosons, defined as $x_{1,2} = 2E_{1,2}/\sqrt{s}$. To obtain the differential cross section with respect to the invariant mass m_{hh} of the two Higgs bosons, we performed a change of integration variables.

The polarization of the initial electron-positron beams plays an important role in the process, since it can significantly enhance the production cross section. In the particular case of the process $e^+e^- \to Zhh$, the tree-level polarized cross section can be related to the

unpolarized cross section σ_{unpol} as

$$\sigma_{RL} = \frac{4g_R^2}{g_L^2 + g_R^2}\,\sigma_{\mathrm{unpol}} \simeq 1.57\,\sigma_{\mathrm{unpol}}\,, \qquad \sigma_{LR} = \frac{4g_L^2}{g_L^2 + g_R^2}\,\sigma_{\mathrm{unpol}} \simeq 2.43\,\sigma_{\mathrm{unpol}}\,, \qquad (21)$$

where $\sigma_{RL,LR}$ refers to 100% right(left)-handed polarized electrons and 100% left(right)-handed polarized positrons, and $g_{L,R}$ are the left (right) couplings of the electrons to the Z boson, i.e. $g_L = -1/2 + s_{\mathrm{w}}^2$ and $g_R = s_{\mathrm{w}}^2$. The same-polarization cross sections σ_{RR} and σ_{LL} are zero because the spin of the e^+e^- pair must add up to one to produce a Z boson in the s-channel. The derivation of the expressions in Eq. (21) can be found in App. A.

In the case of partially-polarized e^-e^+ beams, the cross section is given by [94]

$$\sigma(P_{e^-}, P_{e^+}) = \frac{1}{4}\Big[\,(1 + P_{e^-})\,(1 - P_{e^+})\,\sigma_{RL} + (1 - P_{e^-})\,(1 + P_{e^+})\,\sigma_{LR}\,\Big]\,, \qquad (22)$$

where P_{e^-,e^+} denotes the electron and positron polarization, respectively. The baseline design for the ILC foresees a maximum polarization of $|P_{e^-}| = 80\%$ for electrons and $|P_{e^+}| = 30\%$ for positrons [36]. The possible two beam polarizations with opposite sign yield the following cross sections,

$$\sigma(-80\%, +30\%) = 0.035\sigma_{RL} + 0.585\sigma_{LR} \simeq 1.476\,\sigma_{\mathrm{unpol}}\,, \qquad (23)$$
$$\sigma(+80\%, -30\%) = 0.585\sigma_{RL} + 0.035\sigma_{LR} \simeq 1.004\,\sigma_{\mathrm{unpol}}\,, \qquad (24)$$

where we have used $s_{\mathrm{w}}^2 = 1 - (m_W/m_Z)^2 \simeq 0.223$, with the values of m_W and m_Z from Ref. [67]. The consideration of the beam polarization constitutes one key difference with respect to the tree-level analysis of Ref. [35], where only unpolarized cross sections for the di-Higgs production were considered. The foreseen ILC operating stages relevant for our work, and the corresponding polarized and unpolarized cross section prediction in the SM, can be found in Tab. 3.

The total widths for the H and A Higgs bosons also enter in the total cross section production. We compute them with the public code HDECAY. Furthermore, we have included the effect of one-loop corrected THCs in the allowed Higgs-to-Higgs decays, i.e. for $h \to AA$, $H \to AA$ and $H \to hh$. For instance, for a generic Higgs-to-Higgs decay $\phi \to \chi\chi$, we rescale the partial decay width as

$$\Gamma^{(1)}(\phi \to \chi\chi) = \left(\frac{\lambda_{\phi\chi\chi}^{(1)}}{\lambda_{\phi\chi\chi}^{(0)}}\right)^2 \Gamma^{(0)}(\phi \to \chi\chi)\,, \qquad (25)$$

where we take the one-loop THC $\lambda_{\phi\chi\chi}^{(1)}$ from the effective potential approach (see Sect. 2.2). The change of these partial widths implies also a change in the total width of the ϕ boson. We refer to this "corrected" decay width as $\Gamma_\phi^{\mathrm{corr}}$, and it can be derived from the original decay width Γ_ϕ as

$$\Gamma_\phi^{\mathrm{corr}} = \Gamma_\phi + \sum_\chi \left[\Gamma^{(1)}(\phi \to \chi\chi) - \Gamma^{(0)}(\phi \to \chi\chi)\right]\,. \qquad (26)$$

In this way, we include the main scalar corrections to double Higgs production cross section also in the decay width of the Higgs bosons.

$\sqrt{s}$ [GeV]	$\mathcal{L}_{\text{int}}$ [fb^{-1}]	$\sigma_{\text{SM}}(-80\%, +30\%)$ [fb]	$\sigma_{\text{SM}}(+80\%, -30\%)$ [fb]	Zhh events
500	1600×2	0.232	0.158	$371 + 253$
1000	3200×2	0.177	0.121	$566 + 387$

Table 3: SM prediction for $e^+e^- \to Zhh$ for the foreseen ILC operating phases with beam polarization $P_{e^-} = \mp 80\%$ and $P_{e^+} = \pm 30\%$ [36, 49]. The "$\times 2$" in the second column refers to the sum of the two polarizations, corresponding to the sum in the last column.

It is important to keep in mind that in the alignment limit the only possible BSM effect that one can expect in our computation arises entirely from the one-loop contributions to the coupling λ_{hhh}. Even if the coupling $\lambda_{hhH}^{(1)}$ is different from zero in the alignment limit, which is possible in general, the coupling HZZ is always zero (see Eq. (2)). A complete one-loop computation would also include a BSM effect from the H-mediated diagram involving a one-loop corrected HZZ coupling. In consequence, only at the two-loop level a non-vanishing H-resonance production can be generated in the exact alignment limit, as it involves a one-loop correction to λ_{hhH} as well as the loop-corrected HZZ coupling.

4.2 Benchmark Points

To study the effect of the one-loop corrected THCs we defined specific benchmark points (BPs) that exhibit an interesting phenomenology while being in agreement with the current constraints as described in Sect. 3.1. The input parameters for these BPs are summarized in Tab. 4. We also show their predicted tree-level and one-loop THCs, and the tree-level and "corrected" H width Γ_H^{corr} (see Eq. (26)).[3]

BPal (benchmark point alignment) is the only point valid in all four Yukawa types. It is defined in the alignment limit ($c_{\beta-\alpha} = 0$), and it predicts a large value of κ_λ at one-loop level, due to the large splitting between $m_A = m_{H^\pm}$ and $m_H = \bar{m}$ (see Sect. 3). This BP is chosen specifically to demonstrate the important effects of the one-loop corrections to κ_λ alone on the di-Higgs production cross section. Additionally, BPal constitutes a good reference point to compare results of the cross section predictions considering the one-loop corrected coupling $\kappa_\lambda^{(1)}$ computed by means of the effective potential against the full diagramatic computation (see Sect. 2.2 for more details). This allows us to estimate the importance of the finite-momentum effects in the one-loop corrections to κ_λ, which are neglected in the effective potential approach.

The other points, named BP1, BP2, BP3, BPsign and BPext, are chosen to illustrate interesting phenomenology involving the coupling λ_{hhH} at one-loop level and, consequently, the H resonant peak. Focusing on the ILC with a center-of-mass energy of 500 GeV (ILC500), we consider BPs with masses for the H boson between $2m_h \sim 250$ GeV and $\sqrt{s} - m_Z \sim 409$ GeV, such that the H boson can be produced on-shell. All these points have a value of $|c_{\beta-\alpha}| \geq 0.1$, to ensure a relatively large coupling $ZZH \propto c_{\beta-\alpha}$, to yield a relevant effect from the H resonance. Taking into account current experimental constraints points with such large values of $|c_{\beta-\alpha}|$ are only allowed in the 2HDM Yukawa type I.

---

[3]The A resonance does not play an important role in any of the studied BPs, so for brevity we do not show the predictions for the total width of A.

Point	m_H	m_A	$m_{H^\pm}$	$\tan\beta$	$c_{\beta-\alpha}$	$\bar{m}$	$\kappa_\lambda^{(0)}$	$\kappa_\lambda^{(1)}$	$\lambda_{hhH}^{(0)}$	$\lambda_{hhH}^{(1)}$	Γ_H	Γ_H^{corr}
BPal*	400	800	800	3.0	0.00	400	1.00	5.75	0.00	0.01	0.484	0.485
BP1	300	650	650	12	0.12	300	0.95	4.69	0.02	0.21	0.120	0.319
BP2	350	600	350	5.0	0.12	330	0.87	1.33	0.18	0.33	0.362	0.739
BP3	300	100	300	2.5	-0.18	300	1.06	1.40	0.24	0.44	15.7	16.3
BPsign	350	650	650	20	0.10	350	0.995	5.47	-0.08	0.16	0.175	0.275
BPext	260	700	700	8.0	0.10	260	0.96	5.81	0.07	0.24	0.059	0.189

Table 4: Benchmark points studied in this work to illustrate relevant one-loop effects from triple Higgs couplings. The asterisk (*) indicates that BPal is allowed in the four 2HDM types, while the others are only allowed in the 2HDM type I. Mass-dimension parameters are given in GeV.

Each of these points is chosen to illustrate different aspects of the phenomenology. BP1, BP2 and BP3 are chosen such that their one-loop prediction $\lambda_{hhH}^{(1)}$ is substantially larger than the tree-level prediction $\lambda_{hhH}^{(0)}$. In particular, BP1 has a value for $\lambda_{hhH}^{(0)} \sim 0.02$ (slightly outside the alignment limit), while the one-loop prediction is $\lambda_{hhH}^{(1)} \sim 0.2$. For BP2, the one-loop prediction $\lambda_{hhH}^{(1)}$ is about twice as large as the tree-level prediction $\lambda_{hhH}^{(0)}$. This is also the case for BP3, but in addition the decay width of H is significantly larger than for the other BPs, due to the kinematically allowed decay $H \to AA$, and therefore the H resonant peak is expected to be broader. The point BPsign is chosen because it exhibits a sign change in λ_{hhH}: the one-loop corrected coupling $\lambda_{hhH}^{(1)}$ has a positive sign, while the tree-level prediction $\lambda_{hhH}^{(0)}$ is negative. The final point BPext (benchmark point extreme) features a large enhancement for κ_λ and λ_{hhH} at one loop level, together with a very light H boson close to the production threshold. Therefore, we expect BPext to have a very large cross section, close to the maximum cross section allowed by the current constraints.

It should be noticed that the values of $\lambda_{hhH}^{(1)}$ predicted by our BPs are far from the extremal values discussed in Sect. 3. This is related to the fact that we are focusing on the low-m_H region of the 2HDM, while the larger values for λ_{hhH} (at tree and one-loop level) are found for a heavy H boson.

4.3 Experimental Sources of Uncertainty for the Access to THCs

4.3.1 Detection of the Final $Z + 4b$ Events

In this work we focus on the main decay channel of the SM-like Higgs boson into bottom quarks, i.e. we consider the process $e^+e^- \to Zhh \to Zb\bar{b}b\bar{b}$. Therefore, the experimental signature consists of four b-flavored jets and a Z boson. We estimate the expected number of final $Z + 4b$ events by considering the following reduction factors,

$$\bar{N}_{Z4b} = N_{Zhh} \times \left(\text{BR}\left(h \to b\bar{b}\right)\right)^2 \times \mathcal{A} \times \epsilon_b \equiv N_{Z4b} \times \mathcal{A} \times \epsilon_b, \tag{27}$$

where N_{Zhh} is the number of Zhh events predicted by the cross section computed as detailed in Sect. 4 and $\text{BR}\left(h \to b\bar{b}\right)$ is the branching ratio of the decay $h \to b\bar{b}$ predicted in the 2HDM. To obtain the number of $Z + 4b$ events we consider the luminosities in Tab. 3. The b-tagging

efficiency of detecting the 4 final b-jets is denoted by ϵ_b, where we use $\epsilon_b = 0.85$, following Refs. [40, 95]. In these works it was shown that this choice leads to an optimal Higgs mass resolution in the $Zhh \to q\bar{q}b\bar{b}b\bar{b}$ channel. The detector acceptance is denoted by $\mathcal{A}$, which we estimate by simulating the process $e^+e^- \to Zhh$ with the subsequent decay $h \to b\bar{b}$, and considering the following preselection cuts on the final particle states,

- $E_b > 20$ GeV: At future e^+e^- colliders, the energy of hadronic jets will be reconstructed applying Particle Flow calorimetry techniques [96]. Despite the improvement w.r.t. traditional calorimetry, the energy resolution diminishes rapidly for energies below 20–30 GeV.

- $|\eta_b| < 2.5$ and $|\eta_Z| < 2.5$, where η is the pseudo-rapidity. Final state particles which are very collimated with the e^+e^- beams, would be impossible to detect. It is expected that final states can be reconstructed with Particle Flow calorimetry techniques until polar angles of around 10° [96], which corresponds to a pseudo-rapidity of approximately 2.5.

- $y_{bb} > 0.0025$ at $\sqrt{s} = 500$ GeV and $y_{bb} > 0.0010$ at $\sqrt{s} = 1$ TeV, with $y_{ij} = 2\min\left(E_i^2, E_j^2\right)\left(1 - \cos\theta_{ij}\right)/s$, where θ_{ij} is the angle between the momenta of the particles i and j. The variable y_{ij} is a definition of the distance between particles, which is widely used at e^+e^- colliders to perform the jet clustering procedure via the Durham algorithm [97]. In our analysis, we impose a minimum separation between the final state b jets, in order to be correctly identified as jets. Similar cuts on y_{bb} have been considered in experimental analyses at the ILC with $4b$ jets as final state at 500 GeV [98–100].

The acceptance is estimated as the ratio of events with and without the above cuts,

$$\mathcal{A} = \frac{N^{\text{w/ cuts}}}{N^{\text{w/o cuts}}}.\tag{28}$$

We computed the number of final events with and without cuts for the process $e^+e^- \to Zhh \to Zb\bar{b}b\bar{b}$ with `MadGraph5_aMC v2.9.17` [101] at the parton level and hence did not consider any hadronization of the b-jets. In an experimental analysis, further cuts on the invariant mass of b jet pairs would be considered to reconstruct the Higgs boson h, which can be challenging due to the finite detector resolution. However, we did not consider such cuts, since our simulations are only at the parton level, and thus the vast majority of simulated events shows a pronounced h peak at 125 GeV, unaffected by the detector resolution.

The acceptances for the considered BPs and for the SM case (for comparison) are shown in Tab. 5 for center-of-mass energies of $\sqrt{s} = 500$ GeV and $\sqrt{s} = 1$ TeV. In the 500 GeV case we obtain acceptances around 73% for all considered BPs, which is very close to the acceptance obtained in the SM. In the case of a 1 TeV collider, the acceptances of the studied BPs are between 64% and 73%, which are slightly worse compared to the acceptance obtained in the SM of 76%. We found that the cut on the "distance" between b-jets, y_{bb}, is the cut that reduces the most the number of events yielding $\bar{N}_{Z4b}$.

The fraction of events obtained after the b-tagging reconstruction and the preselection cuts, i.e. $\bar{N}_{Z4b}/N_{Z4b} = \mathcal{A} \times \epsilon_b$, is about 62% at 500 GeV and between 54% and 62% at 1 TeV. The 500 GeV case is in good agreement with the results of the experimental analysis in

	SM	BPal	BP1	BP2	BP3	BPsign	BPext
$\sqrt{s} = 500$ GeV	0.736	0.743	0.739	0.733	0.738	0.741	0.745
$\sqrt{s} = 1000$ GeV	0.758	0.652	0.645	0.689	0.726	0.657	0.641

Table 5: Acceptances for the considered benchmark points (BPs) after the preselection cuts.

Ref. [40].[4] In that work, after their preselection cuts they retain 61.6% of the total predicted $Zb\bar{b}b\bar{b}$ events, after studying the Z decay channels to e^+e^-, $\mu^+\mu^-$, $\nu\bar{\nu}$ and $q\bar{q}$ separately.[5] In addition, they consider more cuts to further suppress the SM background (where ZZZ and ZZh are the most challenging ones) with respect to the Zhh signal. These additional cuts are more severe and only 17.0% of the $Zb\bar{b}b\bar{b}$ events survive them. However, we only consider the events after the simple preselection cuts and b-tagging identification, since a realistic experimental analysis including backgrounds is beyond the scope of this work.

4.3.2 Smearing and Binning of the Cross Section Distributions

The experimental measurements of the invariant mass distributions are affected by the finite resolution of the hadronic calorimeters. Additionally, pairing the final state four b-jets to reconstruct the two SM-like Higgs bosons introduces an extra source of experimental uncertainty. To account for this, we apply an artificial smearing to the theoretical predictions for m_{hh}, assuming Gaussian uncertainties. The smearing is characterized by a percentage, $p\%$, such that each value of m_{hh} in the distribution has an associated Gaussian uncertainty with a full-width at half maximum (FWHM) defined as $p\%$ of m_{hh}. In other words, the FWHM of the Gaussian distributions is given by FWHM $= 2\sqrt{2\log 2}\,\sigma = m_{hh} \times p\%$, where σ is the standard deviation of the distribution.

Currently, the expected experimental resolution on the invariant mass of the final-state Higgs pair at the ILC is unclear. In consequence, we will consider different values for the smearing parameter, namely 0% (no smearing), 2%, 5% and 10% in order to give a notion of the required experimental resolution to access possible BSM signals from THCs at future high-energy e^+e^- colliders. Very recently, there has been progress in the achievable m_{hh} resolution at a high-energy e^+e^- collider operating at 500 GeV [39, 104]. In these preliminary results, the authors find a 1σ uncertainty on m_{hh} of 2.1% in the $Zhh \to \mu^+\mu^- b\bar{b}b\bar{b}$ channel and 2.6% in the $Zhh \to \nu\bar{\nu}b\bar{b}b\bar{b}$ channel, while they remark that there is still room for further improvements. These values would correspond to a smearing of 4.9% and 6.1%, respectively, thus our 5% smearing scenario would represent the most realistic assumption given these results.

Another important aspect in the reconstruction of the differential cross section in terms of m_{hh} is the determination of the bin size in the distribution. A smaller bin size is desirable, as it allows for a more detailed reconstruction of the differential distributions. However, the bin size strongly depends on the number of final events detected at the collider. To determine

---

[4]To our knowledge, there is no analysis at $\sqrt{s} = 1$ TeV for the double Higgs-strahlung channel which we could compare our results to.

[5]There is currently intense progress to update the experimental projections of Ref. [40]. See for instance Refs. [102, 103], where they expect sizable improvements in the projected accuracy in the measurement of $\sigma(Zhh)$ and λ_{hhh} due to better jet tagging, particle identification and the usage kinematic fitting.

the bin size after smearing, we require that each bin in the kinematically allowed region $(2m_h < m_{hh} < \sqrt{s} - m_Z)$ contains at least two reconstructed events, i.e. $\bar{N}_{Z4b} \geq 2$. This approach may be somewhat conservative, as a larger number of events is expected somewhat above the production threshold $(m_{hh} \gtrsim 2m_h)$ compared to the distribution tails $(m_{hh} \sim 2m_h$ and $m_{hh} \lesssim \sqrt{s} - m_Z)$. As a result, the resolution could potentially be higher in the more relevant region, particularly around $m_{hh} \sim m_H$.

5 Sensitivity to One-Loop THCs at e^+e^- Colliders

In this section we analyze the potential sensitivity to the (one-loop corrected) THCs at e^+e^- colliders. We employ the differential distributions of the invariant mass of the final-state di-Higgs pair, m_{hh}, which are shown to be sensitive to the effects of THCs (see Ref. [35] and references therein). As discussed in Sect. 4, the effects of $\kappa_\lambda^{(1)}$ enter via a non-resonant diagram mediated by h-exchange, while the effects of $\lambda_{hhH}^{(1)}$ enter via a resonant diagram mediated by H-exchange. Furthermore, in the analysis presented in this section, we consider the relevant experimental factors that can potentially degrade the experimental measurement of the Zhh distributions, as discussed in Sect. 4.3, and consequently reduce the projected sensitivity to the THCs. To explore all these effects, in this section we show the 2HDM prediction of the m_{hh} distributions for the BPs defined in Tab. 4, which are chosen to exhibit a variety of phenomenological effects that can potentially be expected at a high-energy e^+e^- collider, such as the ILC.

5.1 Sensitivity to the SM-like THC λ_{hhh}

5.1.1 General Impact on the Invariant Mass Distributions

In Fig. 2 we display the differential distribution of the cross section with respect to the invariant di-Higgs mass m_{hh} for center-of-mass energies of 500 GeV (left) and 1 TeV (right) for BPal, see Tab. 4. The polarization has been chosen as $P_{e^-} = -80\%$ and $P_{e^+} = +30\%$. The solid blue lines show the cross section $\sigma_{\text{Eff.Pot.}}^{(1)}$ including the one-loop corrected value of κ_λ from the effective potential. The dashed red lines show the cross section $\sigma_{\text{diag.}}^{(1)}$, which includes the fully diagrammatic one-loop result for κ_λ (which will be discussed in the next subsection). For comparison, the tree-level cross section for the 2HDM, $\sigma_{2\text{HDM}}^{(0)}$, is plotted with solid yellow lines, while the tree-level result for the SM, $\sigma_{\text{SM}}^{(0)}$, is plotted with black dotted lines. This benchmark point has been chosen specifically to demonstrate the effects that the one-loop corrections to λ_{hhh} alone can have on the di-Higgs production cross section. Since the alignment limit $(c_{\beta-\alpha} = 0)$ is assumed for this benchmark point, BSM physics can only enter via the one-loop corrections to $\kappa_\lambda^{(1)}$ (see also the discussion in Sect. 4).

BPal predicts a one-loop corrected triple Higgs coupling $\kappa_\lambda^{(1)} = 5.75$ as given by the one-loop effective potential, which is close to the maximum allowed values for $\kappa_\lambda^{(1)}$ shown in Tab. 2. This means that we have a large deviation from the tree-level prediction $\kappa_\lambda^{(0)} = 1$ as given in the alignment limit. This change in the value of κ_λ is reflected in a strong enhancement of the di-Higgs production cross section, as can be seen in Fig. 2. The cross section including the one-loop corrected $\kappa_\lambda^{(1)}$ is 5.9 (4.8) times larger than the tree-level
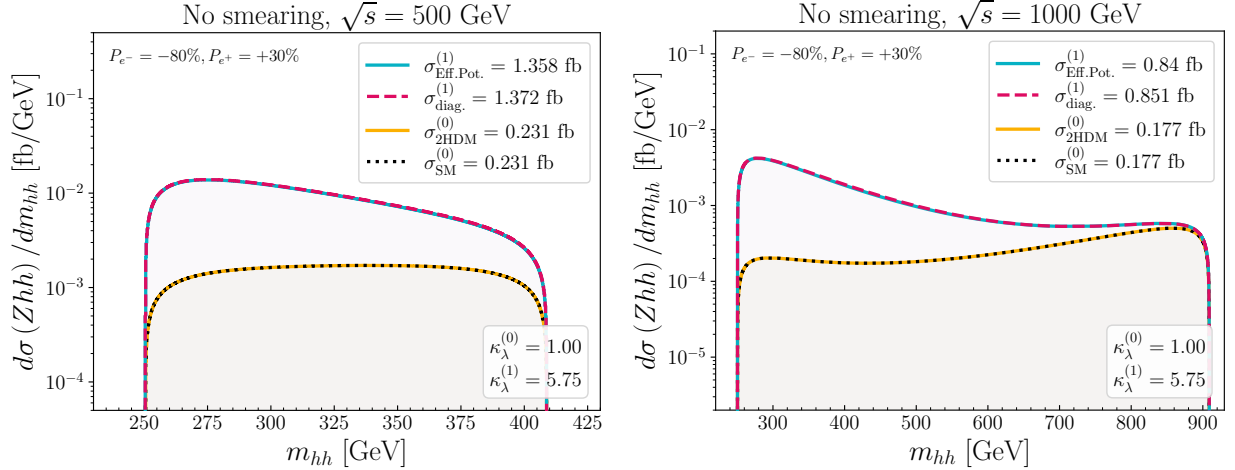
Figure 2: Differential distribution w.r.t. m_{hh} for BPa1 at $\sqrt{s} = 500$ GeV (left) and $\sqrt{s} = 1$ TeV (right) for $P_{e^-} = -80\%$ and $P_{e^+} = +30\%$. The blue lines include the one-loop values of $\kappa_\lambda^{(1)}$ from the effective potential, the dashed red lines include the full diagrammatic prediction for $\kappa_\lambda^{(1)}$, the yellow lines show the 2HDM tree-level prediction and the dotted black lines show the SM tree-level prediction.

prediction at $\sqrt{s} = 500$ (1000) GeV. This enhancement is most pronounced in the low m_{hh} region for both center-of-mass energies, which is known to be the most sensitive region to the variation of κ_λ (see Ref. [35] and references therein). These one-loop corrections to the Zhh cross section induced by $\kappa_\lambda^{(1)}$ are considerably larger than those expected in the SM, which are not larger than 10% for 500–1000 GeV center-of-mass energies [105, 106].

It should be noted that this large increase in the Zhh production cross section happens in the alignment limit (i.e. $c_{\beta-\alpha} = 0$). In the alignment limit the Higgs boson h has production rates and decay branching ratios very similar to those predicted in the SM, therefore a BSM signal for this BP is unlikely to be detectable in single Higgs production at the HL-LHC [45, 107]. This makes di-Higgs production a key process to investigate possible BSM effects and it is crucial to fully test the nature of the Higgs potential.

Regarding the potential experimental sensitivity to κ_λ, the analyses of Refs. [39, 40, 43, 44, 108] show the projections of the expected precision of the measurement of κ_λ at e^+e^- colliders in the case that the SM prediction is not realized, i.e. $\kappa_\lambda \neq 1$. These results are obtained after extrapolating the full simulation results from the SM case, which leads to a determination of κ_λ with an accuracy of 15% at the ILC operating at 550 GeV with an integrated luminosity of 4.4 ab^{-1} [39, 108]. Considering a possible luminosity upgrade of 8 ab^{-1}, the accuracy for $\kappa_\lambda = 1$ drops to 11%. Assuming that integrated luminosity, Ref. [39] gives a very similar projected precision of about 10% in the case that $\kappa_\lambda > 1$ for the Zhh production channel. The combination with the $\nu\bar{\nu}hh$ channel would result in a precision of about 8% for $\kappa_\lambda \geq 1$ at 550 GeV and 8 ab^{-1}. Here it is important to note that the analysis in this subsection only takes into account the theoretical differential distributions, i.e. we do not consider the smearing or binning as discussed in Sect. 4.3. However, the sensitivity to κ_λ discussed above already takes such effects into account, as it is based on ILC experimental analyses. This will be different in Sect. 5.2, where smearing and binning have a crucial effect

on the potential experimental sensitivity on λ_{hhH}.

On more general grounds, since in the 2HDM we mainly find values of $\kappa_\lambda^{(1)} \gtrsim 1$, we conclude that the experimental determination of this coupling via di-Higgs production at e^+e^- colliders would be of about 10% independently of the value realized for $\kappa_\lambda^{(1)}$ (if other BSM effects are negligible), which presents this channel as a great opportunity to determine the Higgs boson self-coupling. It should be mentioned that if an H resonance peak is realized in the m_{hh} distributions, especially close to the production threshold, this could potentially degrade the experimental sensitivity to κ_λ discussed above. In such a case, it would be necessary to efficiently disentangle the contributions of the H resonance from the non-resonant contribution mediated by the h exchange. In the next sections we discuss the potential sensitivity to the H peak at e^+e^- colliders, but we do not analyze this scenario where the effects of λ_{hhH} and κ_λ are mixed (which are beyond the scope of our paper). However, in the case of the discovery of a $\mathcal{CP}$-even resonance around 300 GeV, a detailed experimental analysis would be required.

5.1.2 Finite Momentum Effects from λ_{hhh}

In this subsection we analyze the finite-momentum effects in the loop-corrected trilinear Higgs self-coupling by comparing the effects when using the diagrammatic calculation of $\kappa_\lambda^{(1)}$ to those when using $\kappa_\lambda^{(1)}$ obtained from the effective potential (see the discussion in Sect. 2.2). In Fig. 2 it can be seen that the predictions for $\sigma_{\text{Eff.Pot.}}^{(1)}$ and $\sigma_{\text{diag.}}^{(1)}$ (i.e. the solid blue vs. the dashed red lines) are very close to each other. This implies that the the finite-momentum effects are very small. To test this further, we show in Fig. 3 the result of the fully diagrammatic computation of $\kappa_\lambda^{(1)}$ for BPal as a function of the loop momentum $\sqrt{p^2}$. In the case of di-Higgs production, it corresponds to the invariant mass of the final Higgs pair m_{hh}. The upper (lower) plot shows the real (imaginary) part of the one-loop corrected THC, $\kappa_\lambda^{(1)}$. We also show the prediction from the effective potential with horizontal dashed gray lines. As plot range we have chosen to start at 100 GeV, going up to 900 GeV, i.e. covering the full range that is relevant for $\sqrt{s} = 1000$ GeV. Starting with the real part, for small values of $m_{hh} = \sqrt{p^2}$, the predictions from both approaches are very close to each other. Above $m_{hh} \gtrsim 200$ GeV the real part of $\kappa_\lambda^{(1)}$ obtained with the diagrammatic computation starts deviating more significantly from the prediction of the effective potential, reaching the maximum value of 5.84 at $m_{hh} \sim 400$ GeV. For larger values of m_{hh}, the real part of $\kappa_\lambda^{(1)}$ goes down to ~ 5.6 for $m_{hh} = 1000$ GeV. Concerning the imaginary part of κ_λ, it is negligible below the di-top threshold, and reaches a maximum value of less than 0.3 for the highest values of $\sqrt{p^2} = m_{hh}$. One can see the WW, hh and tt threshold effects at $p = 2m_W$, $2m_h$, $2m_t$, respectively, both in the real and the imaginary parts of $\kappa_\lambda^{(1)}$.[6] The HH threshold is not visible because for this benchmark point λ_{hHH} is proportional to m_h^2/v^2 (see Eq. (13)) and hence very small. The AA and H^+H^- thresholds are present and very prominent as expected given the large values of the hAA and hH^+H^- THCs, but they are at $p = 2m_A = 2m_{H^\pm} = 1600$ GeV, outside the range of the kinematically allowed region for m_{hh}. Our results agree with the corresponding findings in Ref. [17].

---

[6]The ZZ threshold is also present at $2m_Z$, but it is not visible in the plot as its numerical effect is very small.
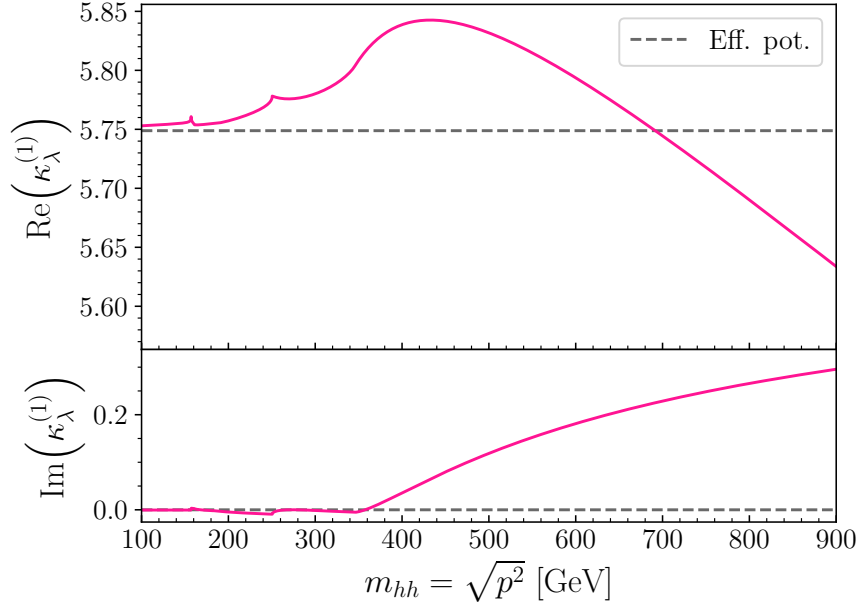
Figure 3: Real (upper) and imaginary (lower) part of the fully diagrammatic one-loop prediction $\kappa_\lambda^{(1)}$ for BPa1 as a function of the invariant mass of the final two Higgs bosons. The gray dashed line shows the respective prediction from the effective potential.

The disagreement between the two computations of $\kappa_\lambda^{(1)}$ shown in Fig. 3 is not large enough to have a phenomenologically relevant impact on the final prediction for the cross section, nor on the m_{hh} predictions, as we have seen also in Fig. 2. In fact, even though it is not visible by eye, the difference between the $\sigma_{\text{Eff.Pot.}}^{(1)}$ and $\sigma_{\text{diag.}}^{(1)}$ has a very similar dependence on m_{hh} as that of $\kappa_\lambda^{(1)}$ in Fig. 3. We can therefore conclude that for the current experimental sensitivities expected at e^+e^- colliders, the simpler $\kappa_\lambda^{(1)}$ calculation using the effective potential is sufficient to capture the relevant one-loop corrections to the total di-Higgs production cross section. Consequently, we will stick to the effective potential calculation in the discussions of the other benchmark points below.

5.2 Sensitivity to the THC λ_{hhH}

The remaining BPs shown in Tab. 4 are specifically chosen to exhibit relevant BSM effects related to the one-loop corrected BSM THC $\lambda_{hhH}^{(1)}$. To assess the potential experimental sensitivity to the triple Higgs coupling $\lambda_{hhH}^{(1)}$ at e^+e^- colliders, we evaluate the statistical significance of the H Higgs boson resonance peak for center-of-mass energies of 500 GeV and 1 TeV. To do this, we perform a profile likelihood analysis exploiting the information of the distributions w.r.t. the invariant mass m_{hh}, following the procedure of Ref. [63] (as detailed below). We use the number of $Z + 4b$ signal events after the preselection cuts and the b-tagging efficiency discussed in Sect. 4.3.1. We also analyze how some sources of uncertainty related to the experimental resolution of the invariant mass distributions affect the statistical significance of the H peaks for our BPs.

5.2.1 Estimation of the Statistical Significance of the H Resonance Peak

In our statistical analysis the signal and background events in the ith bin are given, respectively, by

$$s_i = \bar{N}_{i,4bZ} - \bar{N}^C_{i,4bZ} \,, \tag{29}$$

$$b_i = \bar{N}^C_{i,4bZ} \,, \tag{30}$$

where $\bar{N}_{i,4bZ}$ are the number of $Z + 4b$ events, as discussed in Sect. 4.3.1, and $\bar{N}^C_{i,4bZ}$ are the predicted number of $Z + 4b$ events from the same parameter point but with the THC λ_{hhH} artificially set to zero, corresponding to the events from the "continuum", i.e. without resonance. Consequently, the absolute number of events per bin n_i is given by

$$n_i = s_i + b_i = \bar{N}_{i,4bZ} \,. \tag{31}$$

We test two hypotheses where the expected number of events in the ith bin is given by $E(n_i) = \mu s_i + b_i$, where μ is known as the strength parameter. The value $\mu = 0$ corresponds to the no H resonance hypothesis, while $\mu = 1$ is the nominal signal hypothesis. To test a given value of μ, one can construct the profile likelihood ratio, defined by

$$\lambda(\mu) = \frac{L(\mu)}{L(\hat{\mu})} \,, \tag{32}$$

where $L(\mu)$ is the likelihood function, which is given by the product of the Poisson probabilities of all bins as

$$L(\mu) = \prod_i \frac{(\mu s_i + b_i)^{n_i}}{n_i!} e^{-(\mu s_i + b_i)} \,, \tag{33}$$

i.e. the product of the probabilities of measuring n_i events in the ith bin when $\mu s_i + b_i$ events are expected. The parameter $\hat{\mu}$ in Eq. (32) is the value for the strength parameter that maximizes the likelihood, also known as unconditional maximum-likelihood estimator (MLE). In our case, we consider the simplest case where $\hat{\mu} = 1$, meaning that the measured number of events corresponds exactly to the nominal signal case. This is usually known as a "Asimov" data set, and is typically used to calculate expected sensitivities. Therefore, to compute the significance of the H resonance peak signal, we need the profile likelihood ratio when $\mu = 0$, that is

$$\lambda(0) = \frac{L(0)}{L(1)} \,, \tag{34}$$

such that we test how likely it would be to not measure the signal of H against the scenario with no resonance ($\mu = 0$). To obtain the statistical significance Z we assume that the likelihood in Eq. (32) can be approximated by a Gaussian distribution,

$$Z = \sqrt{-2 \log(\lambda(0))} \,, \tag{35}$$

which is true for a large data sample [63]. With all these expressions we can derive the following formula for the statistical significance:

$$Z = \sqrt{\sum_i (Z_i)^2} \,, \tag{36}$$

where Z_i could be understood as the separate significance of each bin i, given by

$$Z_i = \sqrt{2\left((s_i + b_i)\log\left(1 + \frac{s_i}{b_i}\right) - s_i\right)}. \tag{37}$$

The expression above reduces to the well-known expression for the statistical significance $Z_i \simeq s_i/\sqrt{b_i}$ in the limit $b_i \gg s_i$. It should be noted that with this estimation of statistical significance by means of the profile likelihood ratio, we fully exploit the information of the differential shapes of our invariant mass distributions. More specifically, the H peak shape, which can be realized as a peak-dip or a dip-peak structure, is captured by the fact that the variable s_i in Eq. (29) can be negative.

In this work we consider two scenarios for the initial polarization of the incoming e^+e^- pair, as shown in Tab. 3. Therefore, we can obtain a statistical significance for each initial polarization states $P_{e^-} = \mp 80\%$ and $P_{e^+} = \pm 30\%$, namely Z_{-+} and Z_{+-} respectively. In the following, we will refer to the *combined* statistical significance given by

$$Z = \sqrt{(Z_{-+})^2 + (Z_{+-})^2}. \tag{38}$$

To compute Z_{-+} and Z_{+-} we consider the different bin size expected for each polarization scenarios following the same procedure as discussed in Sect. 4.3.2.

One should keep in mind that a rigorous experimental analysis would be much more complex. For example, a Monte Carlo simulation of the signal and background, together with a full reconstruction of the detector signal, would be required, as well as the consideration of other sources of background (with their corresponding uncertainties), nuisance parameters in the likelihood function, bin-by-bin correlations, etc. Nevertheless, our simplified analysis will shed light on the potential sensitivity to $\lambda_{hhH}^{(1)}$ and to the H resonance peak that can be achieved at e^+e^- colliders under the assumption of negligible background. We hope that it serves as a starting point for future, more complete, experimental analyses.

5.2.2 Access to λ_{hhH} via the H Resonance Peak

In Figs. 4 to 8 we show the differential cross sections for the remaining five BPs displayed in Tab. 4 for $\sqrt{s} = 500$ GeV and $P_{e^-} = -80\%$ and $P_{e^+} = +30\%$. For each benchmark point we present eight plots in two columns. Each row of plots shows the differential cross sections w.r.t. to m_{hh} for different assumptions of smearing, namely a smearing of 0% (no smeared distributions), 2%, 5% and 10%, from top to bottom. The left plots present the theoretical differential distributions[7], while the right plots show the distributions binned such that all bins within the kinematically allowed region have $\bar{N}_{Z4b} \geq 2$. For more details on the smearing and binning of the cross sections see Sect. 4.3.2. Furthermore, in these binned distributions we show $\bar{N}_{Z4b}$ on the right vertical axis. We indicate the minimum required number of events per bin $\bar{N}_{i,Z4b} = 2$ with a horizontal dotted navy line and the kinematically allowed region with two vertical dotted navy lines. In short, the left plots show the theoretical smeared differential cross section of the Zhh process, while the right plots

---

[7]In practice, the differential distributions were obtained by computing the cross section for points separated by 0.2 GeV in the invariant mass.

attempt to replicate the binned distributions that could potentially be measured at an e^+e^- collider. The color labeling and notation for the cross section predictions are the same as in Fig. 2. We additionally include thin dash-dotted lines corresponding to the cross section distributions with the coupling λ_{hhH} artificially set to zero, such that there is no H resonance peak. For those lines the color coding is the same as for the complete distributions. These distributions without the H resonance contribution serve to determine the "background" events b_i discussed in Sect. 5.2.1.

In addition, the plots indicate the statistical significance of the H resonance peak for each assumption of smearing as given by Eq. (38). We remark here that we display the statistical significance after the combination of the two polarization runs considered, as explained in Sect. 5.2.1, even though we only show the cross section distributions for $P_{e^-} = -80\%$ and $P_{e^+} = +30\%$. The upper labels $^{(0)}$ and $^{(1)}$ denote the significance for the H peak for the tree-level and one-loop distributions, respectively. In the case of the tree-level significance, we obtain them with the corresponding size of the bins such that $\bar{N}_{Z4b} \geq 2$, although in the plots, for simplicity, we show the distributions of the tree-level prediction with the bin size determined from the prediction including one-loop THCs. In the plots in the left columns we also provide the significance values for the differential cross section distributions without binning, which we denote as Z_{diff}. With these significance values, we can analyze the impact that the resolution on the invariant mass distributions can have on the potential access to the H resonance peak, and thus the sensitivity to the $\lambda_{hhH}^{(1)}$ coupling, at e^+e^- colliders. We gather all these significance values after the smearing and binning of the distributions in Tab. 6, where we also include the size of the bins given by our prescription for the one-loop and tree-level distributions.

As stated above, here we concentrate on the results for $\sqrt{s} = 500$ GeV. The results for a center-of-mass energy of 1 TeV (i.e. the cross section distributions for the considered BPs and their respective H resonance significance) can be found in App. B. Comparing the 500 GeV and the 1000 GeV results, one can see that the latter do not provide any further qualitative information w.r.t. the 500 GeV case. This is to be expected, since our BPs have been chosen such that an H resonance peak can be observed at $\sqrt{s} = 500$ GeV and the Zhh cross section decreases with $1/s$. Nevertheless, it should be mentioned that a collider operating at $\sqrt{s} = 1$ TeV would be of great importance in both cases where we observe an H resonance or not. In the former case, the 1 TeV machine can help to reduce the statistical and systematic uncertainties in the measured properties of the new scalar, and in the latter case higher center-of-mass energies provide potential access to heavier states. Another advantages of a 1 TeV collider is given by the fact that it would have access to the vector boson fusion production channel, which is not considered in the present work (for more details on this see e.g. Ref. [35] and references therein).

We start the discussion of our results with the distributions for BP1 shown in Fig. 4. We can see an enhancement by a factor of 5.6 in the cross section $\sigma_{\text{Eff.Pot.}}^{(1)}$ with one-loop corrected THCs compared to the tree-level prediction $\sigma_{\text{2HDM}}^{(0)}$. This is partly due to the large value of $\kappa_\lambda^{(1)} = 4.7$ at one loop, which increases the non-resonant contributions to the cross section, similar to the case of BPa1 as described in Sect. 5.1. We now turn to the effect of the one-loop corrections of $\lambda_{hhH}^{(1)}$, which enters the cross section through a resonant diagram mediated by the heavy Higgs boson H. In BP1, the resonance peak is expected at $m_{hh} = m_H = 300$ GeV, as it can be seen in all plots in Fig. 4. Furthermore, it can be seen in
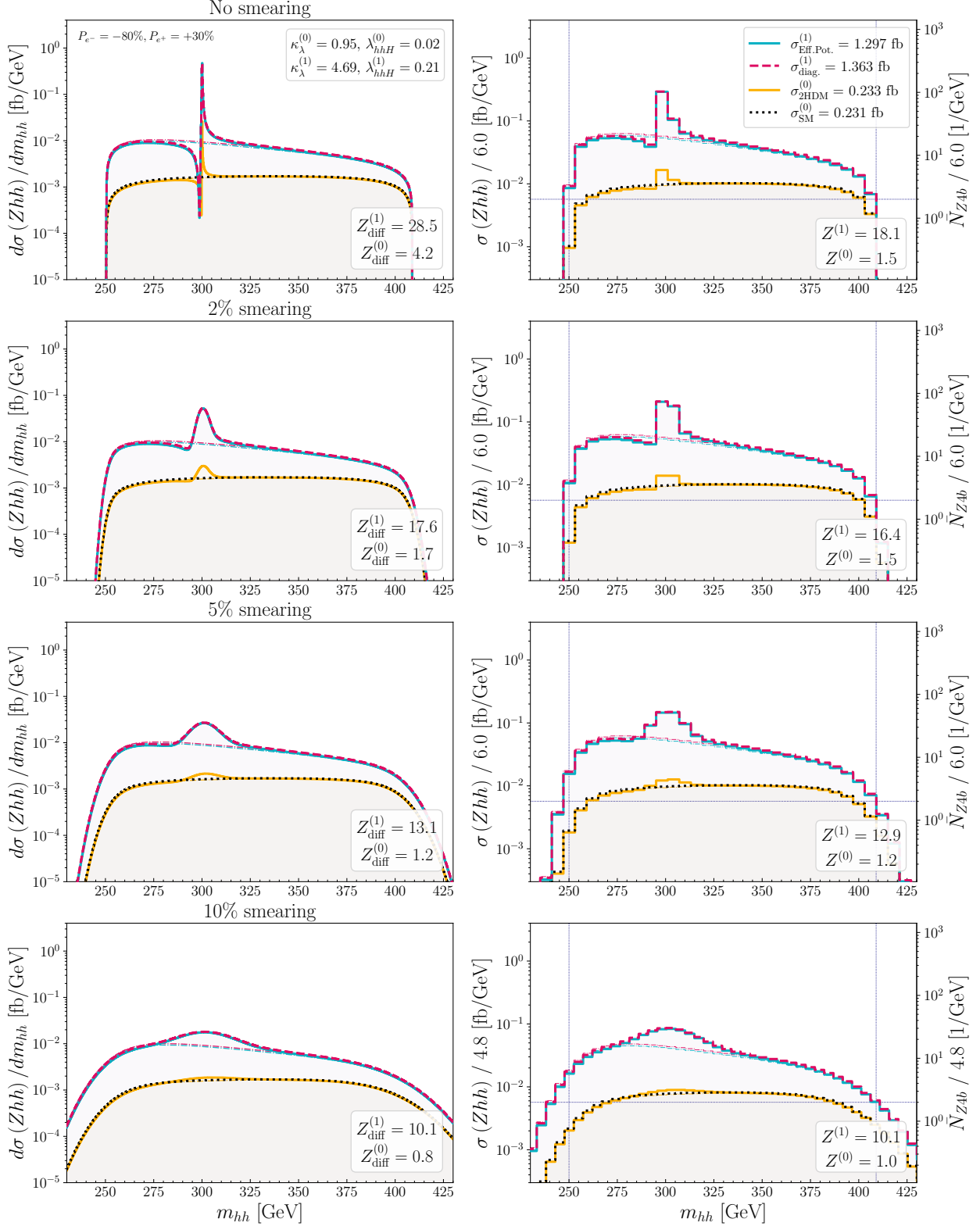
Figure 4: Differential distribution w.r.t. m_{hh} for BP1 at $\sqrt{s} = 500$ GeV for $P_{e^-} = -80\%$ and $P_{e^+} = +30\%$. The color coding is the same as in Fig. 2, and the red and blue lines also include $\lambda_{hhH}^{(1)}$ as predicted by the effective potential. From top to bottom, the distributions have a smearing of 0% (no smearing), 2%, 5% and 10%. The left plots show the theoretical differential distributions, and the right ones show the distributions with a bin size such that all bins inside the kinematically allowed region have $\bar{N}_{i,Z4b} \geq 2$ (dotted navy lines).

24

all plots that the H resonance peak is more prominent, i.e. it is more separated from the non-resonant "continuum" contributions, in the distributions with one-loop THCs compared to ones with the tree-level couplings. This is due to the fact that for our benchmark point the tree-level prediction for λ_{hhH} is very close to zero, while the one-loop correction increases the value of this coupling to a much larger value of $\lambda_{hhH}^{(1)} = 0.21$. This effect can be also quantified by the statistical significance of the differential distributions, $Z_{\text{diff}}^{(1)} = 28.5$ and $Z_{\text{diff}}^{(0)} = 4.2$ in the case of no smearing. For all considered smearing values and bin sizes, we find that the significance with one-loop couplings is roughly one order of magnitude larger than the significance with tree-level couplings. This implies that the λ_{hhH} resonant peak is potentially accessible after considering the one-loop corrections to λ_{hhH}, whereas the tree-level prediction would naively suggest that it is inaccessible.

We can also discuss the effect of the binning size and the smearing on the cross section distributions, and in particular on the significance of the H resonance peak. We find that the smearing has the greater effect on $Z_{\text{diff}}^{(1)}$. The significance decreases from $Z_{\text{diff}}^{(1)} = 28.5$ with no smearing, to $Z_{\text{diff}}^{(1)} = 17.6$ with a 2% smearing, to $Z_{\text{diff}}^{(1)} = 13.1$ with a 5% smearing, to $Z_{\text{diff}}^{(1)} = 10.1$ with a 10% smearing. This loss of sensitivity is also clearly visible in the plots, as the resonant peak becomes less prominent and broader as the smearing percentage increases. Binning the unsmeared distribution also reduces the sensitivity to the H resonance, namely from $Z_{\text{diff}}^{(1)} = 28.5$ down to $Z^{(1)} = 18.1$. However, the significance is not affected in a relevant way by the binning of the distributions when smearing is considered. The reason is that the resonance peak in BP1 is very sharp and narrow, which can only be reconstructed with extremely good experimental resolution. But as soon as the distribution is smeared and the resonance becomes broader, the binning does not reduce the sensitivity to H significantly.

We also find that the smearing and binning of the distributions reduces the potential sensitivity to the sign of λ_{hhH}. The H mediated diagram changes sign exactly at $m_{hh} = m_H$, which results in a change of the interference with the rest of the non-resonant diagrams as well (see for instance [61, 109]). Therefore, one can find the so-called dip-peak or peak-dip structures around the resonant peak depending on the sign of the λ_{hhH} coupling. For BP1, we have a dip-peak structure due to the fact that $\lambda_{hhH} > 0$, as can be clearly seen in the unsmeared differential distribution (top left plot in Fig. 4). However, compared to the binned distribution without smearing (top right plot), an increased smearing results in "losing" the dip structure to the left of the resonance, and only an enhancement to the right is visible. For the 2% smeared distributions, the differential distribution barely shows the dip-peak structure. For larger percentages of smearing there are no traces of any complex structure around the H resonance peak.

We turn to the results obtained for BP2, shown in Fig. 5. For this benchmark point, the tree-level and one-loop predictions for κ_λ are both rather close to 1, and thus the non-resonant contributions in $\sigma_{\text{Eff.Pot.}}^{(1)}$, $\sigma_{\text{diag.}}^{(1)}$ and $\sigma_{\text{2HDM}}^{(0)}$ are rather close to the SM prediction $\sigma_{\text{SM}}^{(0)}$. On the other hand, the one-loop corrections to λ_{hhH} are sizable for this point. In BP2 the one-loop corrected coupling is $\lambda_{hhH}^{(1)} = 0.33$, which is almost twice the tree-level prediction $\lambda_{hhH}^{(0)} = 0.18$. The effect of this change in the value of λ_{hhH} is visible in the resonance peaks of all the plots in Fig. 5, which are found around $m_{hh} = m_H = 350$ GeV. The H resonance peaks are higher in the cross section predictions with the one-loop corrected THCs compared to the tree-level predictions. This effect can be quantified with the change in the statistical significance. In
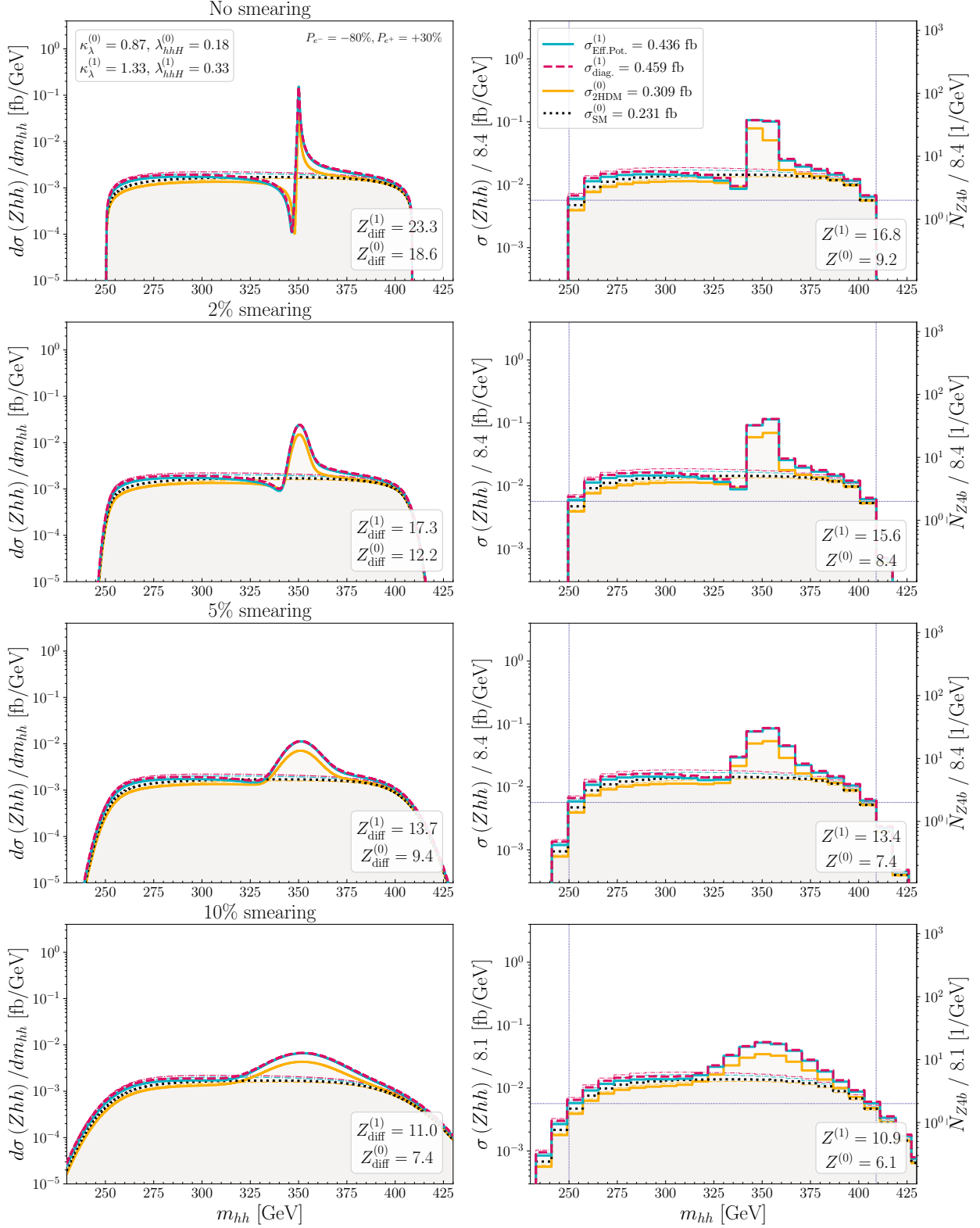
Figure 5: Differential distribution as a function of m_{hh} for BP2 at $\sqrt{s} = 500$ GeV for $P_{e^-} = -80\%$ and $P_{e^+} = +30\%$. The color coding is the same as in Fig. 4.

the unsmeared differential distributions, we find $Z_{\text{diff}}^{(1)} = 23.3$, while $Z_{\text{diff}}^{(0)} = 18.6$. As in BP1, the statistical significance of the H resonance peak decreases when we consider smearing in the differentia distributions. For the largest smearing percentage considered, 10%, but no binning, we find $Z_{\text{diff}}^{(1)} = 11.0$ and $Z_{\text{diff}}^{(0)} = 7.4$. The effect of the binning of the distributions on the significance is similar to that found for BP1. Binning the unsmeared distributions reduces the sensitivity to the H resonance peak, from $Z_{\text{diff}}^{(0)} = 18.6$ to $Z^{(0)} = 9.2$ and from $Z_{\text{diff}}^{(1)} = 23.3$ to $Z^{(1)} = 16.8$. On the contrary, when the distributions are smeared, the subsequent binning does not significantly worsen the statistical significance of the H peak. Consequently, in BP2 the one-loop corrections to λ_{hhH} lead to a modest improvement for the potential sensitivity to the H resonance peak, and hence to the value of λ_{hhH}. The unsmeared and unbinned distributions also exhibit a very clear dip-peak structure, which depends on the sign of λ_{hhH}, as discussed above. However, as with the distributions for BP1, the smearing of the cross section distributions, and to a lesser extent the binning of them, erases any trace of this dip-peak structure, making the experimental access to the sign and size of the λ_{hhH} coupling more challenging.

The differential distributions for BP3 are shown in Fig. 6. For this point the pseudoscalar boson A is light enough that the decay channel $H \to AA$ is kinematically allowed. Consequently, the total decay width of H is relatively large, amounting to $\Gamma_H^{\text{corr}} = 16.3$ GeV after considering the one-loop corrected coupling λ_{HAA} (see Eq. (26)). For comparison, in all other BPs Γ_H^{corr} is always less than 1 GeV. This large value of Γ_H^{corr} is the reason why there is no narrow resonant peak-dip structure around $m_{hh} = m_H = 300$ GeV, in contrast to the other studied points. The large width of H yields a very broad peak-dip structure that extends approximately from the threshold at $m_{hh} = 250$ GeV to $m_{hh} \simeq 350$ GeV. It is furthermore interesting to note that the distributions in the plots exhibit a peak-dip structure, instead of a dip-peak structure as in the previously discussed BP1 and BP2. The reason lies in the choice of $c_{\beta-\alpha} < 0$ in BP3, which changes the sign of the ZHH coupling. Despite $\lambda_{hhH} > 0$ in all BPs, the product $g_{HZZ} \times \lambda_{hhH}$ changes sign w.r.t. the other BPs, and thus changes the global sign of the H-resonance diagram. The absence of a narrow H peak results in a lower statistical significance compared to the other BPs. Specifically, in the unsmeared differential distributions we find $Z_{\text{diff}}^{(1)} = 6.0$ and $Z_{\text{diff}}^{(0)} = 2.9$. The significance is larger after including the one-loop corrected THCs since for this point $\lambda_{hhH}^{(1)} = 0.44$, while $\lambda_{hhH}^{(0)} = 0.24$ (the effect of κ_λ is negligible as it it increases solely by roughly 30% when including the NLO corrections in contrast to an 80% increase in case of the λ_{hhH} coupling), but this enhancement is not sufficient to reach large values of the statistical significance. Smearing and binning of the distributions does not play an important role for BP3, since the differential distributions are already very smooth. For instance, the binning of the unsmeared distribution yields a significance of $Z^{(1)} = 5.7$, and a smearing of 10% yields $Z^{(1)} = 4.6$, very close to the values of the unbinned distribution. For all these reasons, BP3 is a more challenging point to probe at future e^+e^- colliders.

We continue our discussion of the sensitivity to λ_{hhH} via the H resonace diagram with BPsign, whose predicted invariant mass distributions are shown in Fig. 7. BPsign was specifically chosen because the one-loop corrections to λ_{hhH} change the sign of this THC. Specifically, the tree-level prediction is $\lambda_{hhH}^{(0)} = -0.08$, while we at the one-loop level we find $\lambda_{hhH}^{(1)} = 0.16$. As discussed earlier, this changes the shape of the cross section around the resonance peak, which is located at $m_{hh} = m_H = 350$ GeV for this point. The tree-level
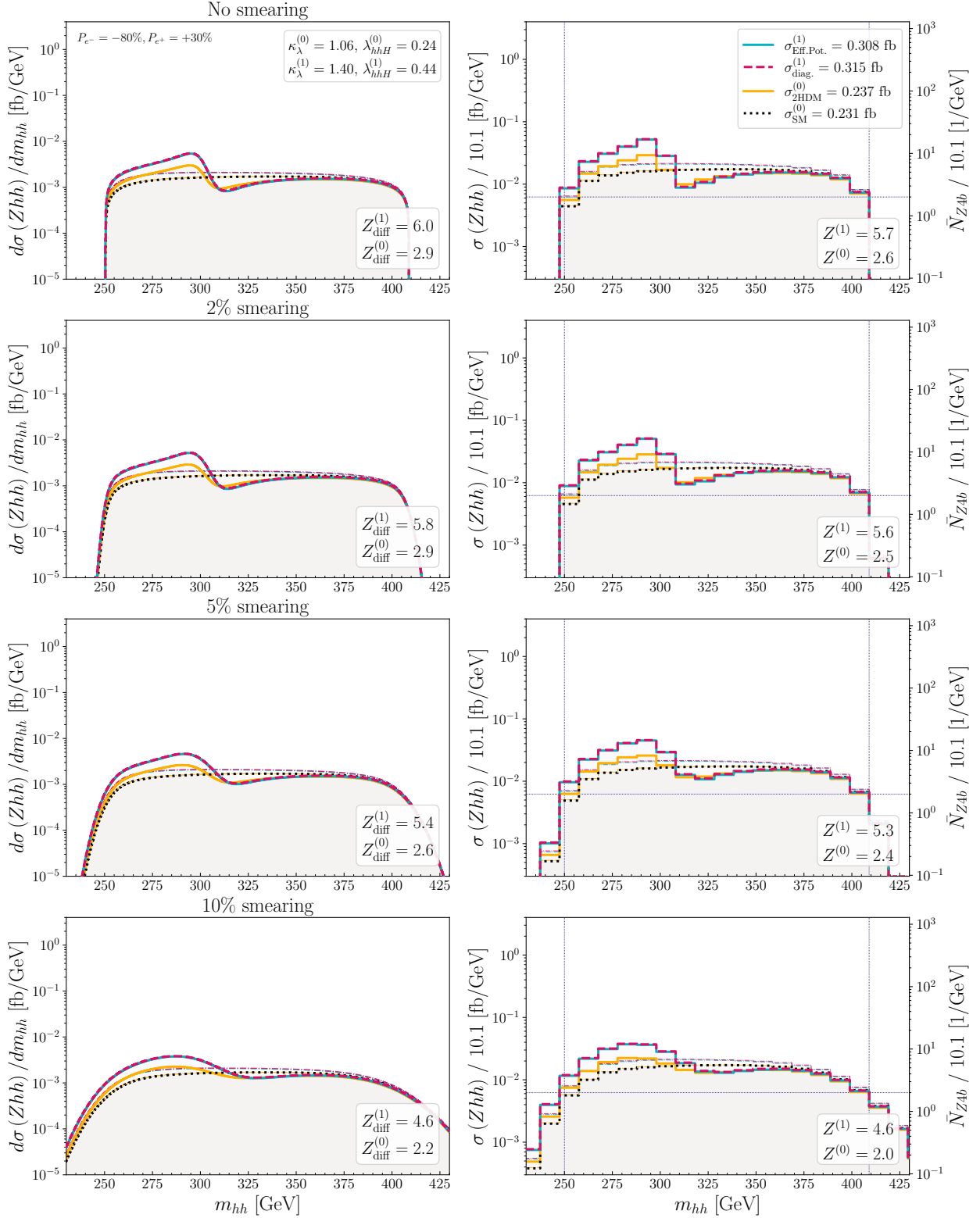
Figure 6: Differential distribution as a function of m_{hh} for BP3 at $\sqrt{s} = 500$ GeV for $P_{e^-} = -80\%$ and $P_{e^+} = +30\%$. The color coding is the same as in Fig. 4.
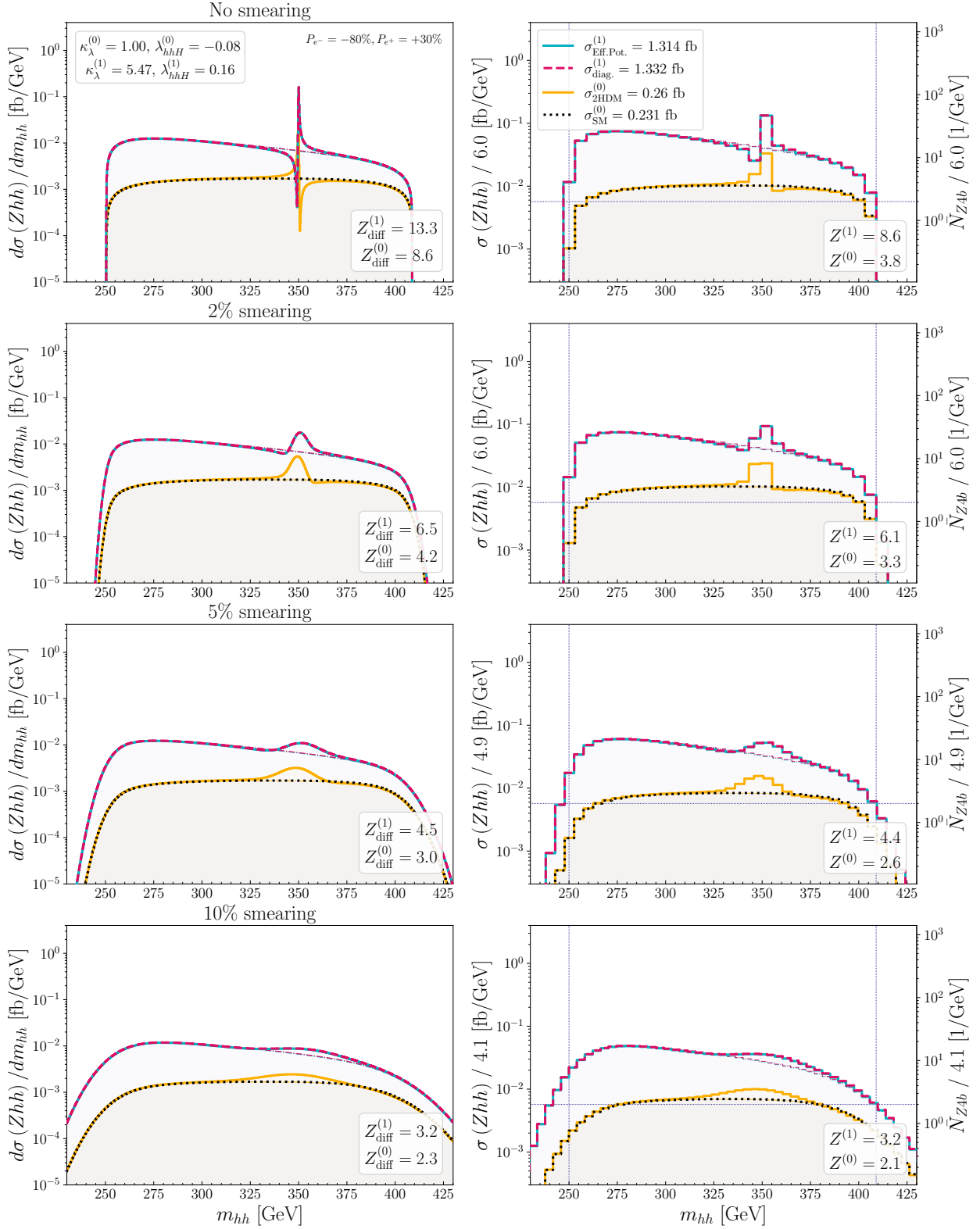
Figure 7: Differential distribution as a function of m_{hh} for BPsign at $\sqrt{s} = 500$ GeV for $P_{e^-} = -80\%$ and $P_{e^+} = +30\%$ The color coding is the same as in Fig. 4.

differential distribution without smearing exhibits a peak-dip structure, which changes to a dip-peak structure once the one-loop corrected THCs are taken into account. The resonance peak also becomes more prominent as the absolute value of $\lambda_{hhH}^{(1)}$ is increased relative to $\lambda_{hhH}^{(0)}$. This is reflected in the statistical significance in both cases: the distribution with one-loop corrections yields a value of $Z_{\text{diff}}^{(1)} = 13.3$, while the tree-level prediction gives $Z_{\text{diff}}^{(0)} = 8.6$. The dip-peak and peak-dip structures of the H peaks are still visible in the binned distributions without smearing, although the significances are reduced to $Z^{(1)} = 8.6$ and $Z^{(0)} = 3.8$. However, any visible hint from the sign of λ_{hhH} via the shape of the H resonance is lost when we consider the smeared distributions, even with the smallest smearing percentage considered of a 2%. Furthermore, the significance is also reduced to roughly half in the differential distributions. As in the previous points analyzed, once the smearing is included in the distributions, the binning of the distribution does not further reduce the statistical significance of the H resonance peak. This implies that the experimental access to λ_{hhH} will require a high resolution in m_{hh}, similar to our findings for the previously discussed BPs. For this point, the one-loop corrections to κ_λ are also considerable, going from $\kappa_\lambda^{(0)} = 1$ to $\kappa_\lambda^{(1)} = 5.47$. Consequently, we observe an overall enhancement in the differential cross sections with one-loop corrected THCs for values of m_{hh} away from the resonance peak around $m_{hh} = m_H = 350$ GeV. This overall enhancement due to a large value of $\kappa_\lambda^{(1)}$ is another factor that can facilitate the experimental access to the H resonance peak, and thus to λ_{hhH}, since it implies more final $Z + 4b$ events.

The differential distributions in m_{hh} for the last considered point BPext ("BP extreme") are shown in Fig. 8. The total cross section with one-loop corrected THCs is with 1.8 fb much larger than the tree-level cross section of 0.3 fb. Given that in BPext the loop-corrected THCs are $\kappa_\lambda^{(1)} = 5.81$ and $\lambda_{hhH}^{(1)} = 0.24$, together with the fact that $m_H = 260$ GeV is very close to the threshold, we find that BPext predicts a total cross section close to the maximum that can be found in the 2HDM for an e^+e^- collider at 500 GeV. This very light heavy $\mathcal{CP}$-even H boson and the large value of $\lambda_{hhH}^{(1)}$ imply a very prominent and large resonance peak at $m_{hh} = m_H$. Such a large H peak results in a large statistical significance of $Z_{\text{diff}}^{(1)} = 32.3$ from the differential cross section taking into account the THCs at the one-loop level. Even after binning the distributions one finds a large significance of $Z^{(1)} = 21.4$. Conversely, the smearing of the distributions has a very large impact on the statistical significance, since the H resonance peak in this point is very narrow. For a smearing of 2%, the significance drops to $Z_{\text{diff}}^{(1)} = 19.4$, for 5% to $Z_{\text{diff}}^{(1)} = 15.5$, and for 10% to $Z_{\text{diff}}^{(1)} = 13.5$. Similar to the other points, the binning of the cross section distributions after the smearing does not have a relevant impact on the values obtained for the statistical significance, especially when the smearing is large. Although the significance is reduced by the smearing, the resonance is so pronounced that the statistical significance is $Z^{(1)} = 13.5$ even in the worst case analyzed (10% smearing).

The statistical significances of the H resonance peaks for the studied BPs for all considered values of smearing, with and without binning, are summarized in Tab. 6. This table also includes the bin size (labeled as "Bin") obtained with the method described in Sect. 4.3.2, both for the tree-level and the one-loop corrected differential distributions, and for the two considered polarization running scenarios. For all points considered, the significance obtained from the distributions with one-loop THCs is always larger than that obtained with the tree-level predictions. This is due to two facts: first, our points were chosen
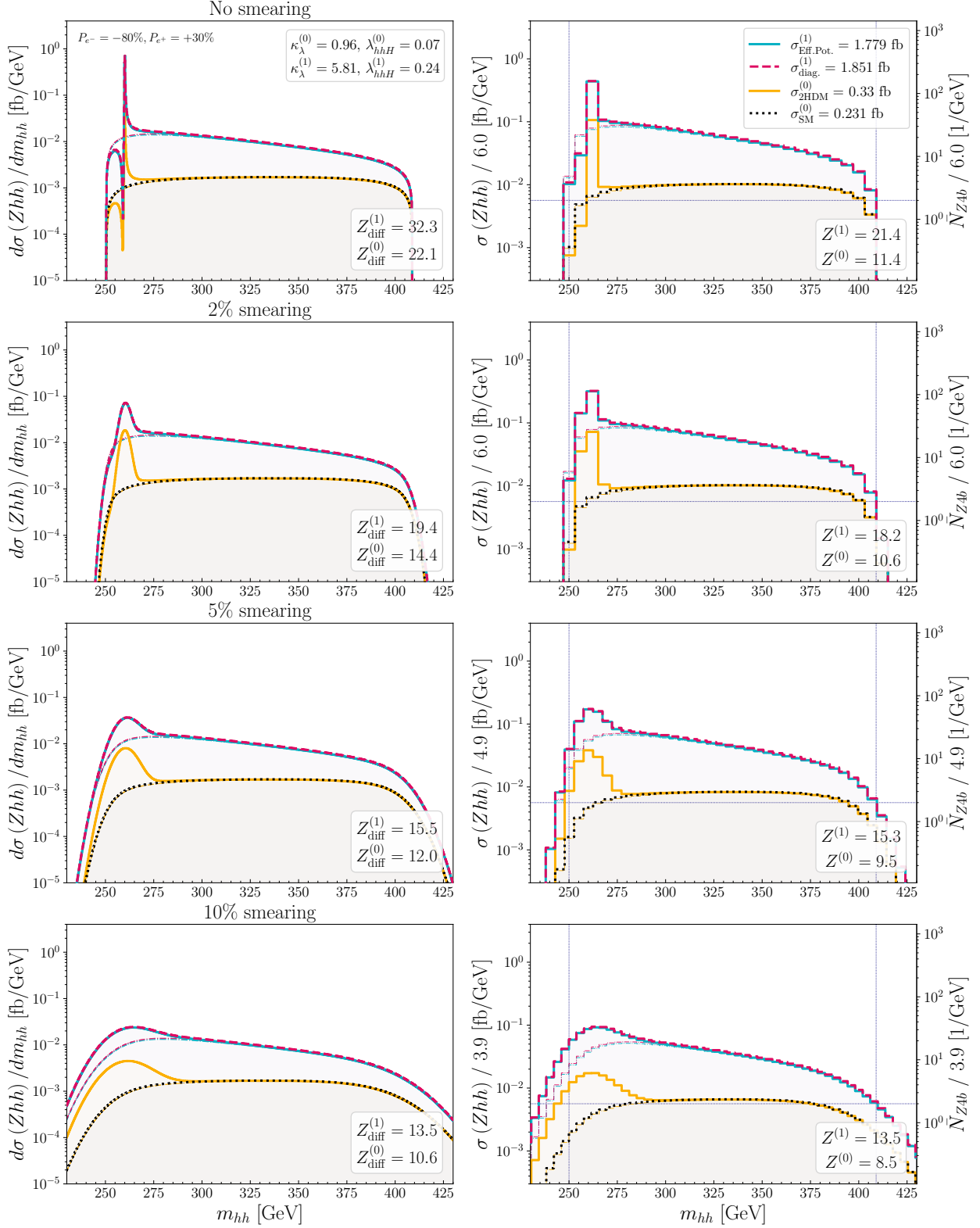
Figure 8: Differential distribution as a function of m_{hh} for BPext at $\sqrt{s} = 500$ GeV for $P_{e^-} = -80\%$ and $P_{e^+} = +30\%$. The color coding is the same as in Fig. 4.

31

Point	Smearing	$\text{Bin}_{-+}^{(1)}$	$\text{Bin}_{+-}^{(1)}$	$Z_{\text{diff}}^{(1)}$	$Z^{(1)}$	$\text{Bin}_{+-}^{(0)}$	$\text{Bin}_{-+}^{(0)}$	$Z_{\text{diff}}^{(0)}$	$Z^{(0)}$
BP1	0%	6.0	7.6	28.5	18.1	11.4	13.3	4.2	1.4
	2%	6.0	7.6	17.6	16.4	11.4	13.3	1.7	1.4
	5%	6.0	7.2	13.1	12.9	11.4	13.3	1.2	1.1
	10%	4.8	6.4	10.1	10.1	10.8	13.3	0.8	0.8
BP2	0%	8.4	12.3	23.3	16.8	11.4	14.9	18.6	11.1
	2%	8.4	12.3	17.3	15.6	11.4	14.9	12.2	10.1
	5%	8.4	12.3	13.7	13.4	11.4	14.9	9.4	9.0
	10%	8.1	11.6	11.0	10.9	10.9	14.9	7.4	7.3
BP3	0%	10.1	15.1	6.0	5.7	10.8	13.3	2.9	2.9
	2%	10.1	15.1	5.8	5.6	10.8	13.3	2.9	2.8
	5%	10.1	15.1	5.4	5.3	10.8	13.3	2.6	2.6
	10%	10.1	14.0	4.6	4.6	10.8	14.8	2.2	2.2
BPsign	0%	6.0	7.6	13.3	8.6	11.4	13.3	8.6	4.3
	2%	6.0	7.6	6.5	6.1	11.4	13.3	4.2	3.8
	5%	4.9	6.5	4.5	4.4	10.8	13.3	3.0	2.9
	10%	4.1	6.0	3.2	3.2	10.8	13.3	2.3	2.2
BPext	0%	6.0	7.6	32.3	21.4	11.4	11.4	22.1	14.3
	2%	6.0	7.6	19.4	18.2	9.5	11.4	14.4	12.8
	5%	4.9	6.0	15.5	15.3	9.5	12.1	12.0	11.8
	10%	3.9	5.6	13.5	13.5	9.3	12.1	10.6	10.5

Table 6: Statistical significance Z for all the benchmark points (BPs) for a center-of-mass energy of $\sqrt{s} = 500$ GeV. Z_{diff} corresponds to the significance obtained from the differential distributions, while Z is the significance considering the corresponding bin size (chosen such that the expected events for the bins within the kinematically allowed area are larger than 2). The upper labels $^{(0)}$ and $^{(1)}$ refer to the significance and bin size including tree-level or one-loop THCs, respectively. The lower labels $_{-+}$ and $_{+-}$ refer to the polarization scenarios with $P_{e^-} = \mp 80\%$ and $P_{e^+} = \pm 30\%$, respectively.

such that $|\lambda_{hhH}^{(1)}| > |\lambda_{hhH}^{(0)}|$, resulting in a more pronounced H resonance peak, and second for some points $\kappa_\lambda^{(1)} > \kappa_\lambda^{(0)}$, which increases the predicted number of final $Z + 4b$ events. Thus, we demonstrated that one-loop corrections to THCs can have a large impact on a phenomenological analyses in di-Higgs production.

The values for the statistical significances allow us to also quantify the potential relative sensitivity to the H resonance peak, which is the main experimental access to the THC λ_{hhH} at e^+e^- colliders. For all points, the larger significance is always given by the unsmeared and unbinned distributions $Z_{\text{diff}}^{(1)}$. This is to be expected, since a differential distributions without smearing yields the purely theoretical prediction for the cross section. In the case that the H peak is narrow, it can only be observed in these theoretical distributions. Correspondingly, after binning, the significance always worsens, especially in the unsmeared case and in the

2% smearing case, or at best remains the same, especially when the smearing is already large (5% or 10%). Smearing also degrades the sensitivity to the H resonance peak, because the larger the smearing, the smaller the significance obtained. However, it should be noted that once the distributions are smeared, the subsequent binning does not have a large impact on the significance. Therefore, from our analysis we conclude that smearing is the limiting factor in the sensitivity to the H resonance peak, and thus to the value of λ_{hhH}. Binning is only important in the case of unsmeared distributions.

It should be noted that we do not consider any experimental backgrounds in our analysis of the significance to the H resonance. Therefore, the significance values given in this section are only accurate in the case that it is possible to efficiently subtract all the background events from the di-Higgs signal. Consequently, our values for the experimental significance to the H peak should be considered as optimistic. Nevertheless, we have decided to not consider any further experimental cuts for our estimation of the final accessible events apart from those discussed in Sect. 4.3.1, since they are based on a non-resonant search for a κ_λ signal. In the case of a resonant search, as in the present study, it is likely that an experimental study follows a different strategy, similar to the di-Higgs resonant and non-resonant searches performed by the ATLAS and CMS collaborations at the LHC. For reference, we show in App. C our prediction for the statistical significance for our BPs, but with only 17% of the theoretical $Zb\bar{b}b\bar{b}$ events, which corresponds to the result of Ref. [40] to suppress the signal vs. background in the Zhh channel in the SM (but based on non-resonant di-Higgs production).

6   Conclusions

In this work we studied the impact of one-loop corrections to triple Higgs couplings (THCs) on di-Higgs production in BSM models with extended Higgs sectors at high-energy e^+e^- colliders. We furthermore explored the experimental sensitivity to THCs and how to access them at e^+e^- colliders. In particular, we focused on the di-Higgs-strahlung process, which is the dominant production channel of two SM-like Higgs bosons for center-of-mass energies between roughly 500 GeV and 1 TeV. In extended BSM Higgs sectors, the main one-loop corrections to this process are expected to be induced by the involved THCs at the one-loop level, due to the large scalar couplings that can be realized in such models [15–17].

As a theoretical framework to explore the effect of one-loop THCs on di-Higgs production, we used the two-Higgs doublet model (2HDM). In our study, we identified the lighter of the two CP-even Higgs bosons, h, with the SM-like Higgs boson observed at the LHC with a mass of ~ 125 GeV. In the 2HDM, the THCs λ_{hhh} and λ_{hhH} enter in the prediction of the cross section via diagrams mediated by the h and the H Higgs boson, respectively. The size of most of the 2HDM scalar couplings involved in these THCs at the one-loop level, namely $\lambda_{hhh}^{(1)}$ and $\lambda_{hhH}^{(1)}$, are constrained only by the unitarity requirement of the model, which allows potentially large one-loop corrections from the scalar sector. We computed the one-loop corrections to these THCs using the Coleman-Weinberg effective potential, and we furthermore compared our results to those of a fully diagrammatic computation of the one-loop corrections to $\lambda_{hhh}^{(1)}$. This allowed us to estimate the importance of the finite-momentum effects in the one-loop corrections to $\lambda_{hhh}^{(1)}$.

The first part of our analysis evaluated the currently allowed ranges for λ_{hhh} (or alterna-

tively $\kappa_\lambda = \lambda_{hhh}/\lambda_{\mathrm{SM}}^{(0)}$) and λ_{hhH}, both at the tree and at the one-loop level, considering all relevant current experimental and theoretical constraints. We found that one-loop corrections can significantly impact the allowed values of $\kappa_\lambda^{(1)}$ and $\lambda_{hhH}^{(1)}$ within the viable 2HDM parameter space, as summarized in Tab. 2. Specifically, $\kappa_\lambda^{(0)}$ is tightly constrained to be close to 1 (i.e. the SM value), due to the necessity to be close to the alignment limit. However, one-loop corrections can enhance its prediction up to ~ 6 in all 2HDM types, even in the alignment limit. For $\lambda_{hhH}^{(0)}$, values around ± 1.5 are allowed at tree level, extending to approximately ± 2 including the one-loop corrections. These large corrections arise from strong couplings of h and H to heavy Higgs bosons, such as A, $H^\pm$, or H itself.

Next, we investigated the potential sensitivity to one-loop corrected THCs at high-energy e^+e^- collider via the double Higgs-strahlung process, i.e. $e^+e^- \to Zhh$. We defined six benchmark points (see Tab. 4) allowed by all current constraints, chosen to exhibit a variety of interesting phenomenology related to THCs. In particular, the benchmark points illustrate how one-loop corrections to THCs can affect the final (absolute and differential) di-Higgs production cross section. We focused on an e^+e^- collider operating at 500 GeV, close to where the maximum production cross section is found in the SM (but we also evaluated results for a center-of-mass energies of 1 TeV in some cases). We also took into account the beam polarization at an e^+e^- collider, with $P_{e^-} = \mp 80\%$ and $P_{e^+} = \pm 30\%$, which enhances the di-Higgs production cross section w.r.t. unpolarized beams. To disentangle the effects of the THCs involved in the process, we studied the differential distributions w.r.t. the invariant mass of the final pair of Higgs bosons, m_{hh}.

The effect of $\kappa_\lambda^{(1)}$ enters via a non-resonant diagram mediated by h, with maximum sensitivity near the threshold at $m_{hh} = 2m_h \simeq 250$ GeV. We found that large values of $\kappa_\lambda^{(1)}$ strongly enhance the production cross section, even in the alignment limit. For our benchmark point BPa1, which predicts $\kappa_\lambda^{(1)} = 5.75$, the di-Higgs production cross-section is enhanced by factors of 5.9 (4.8) at $\sqrt{s} = 500$ (1000) GeV relative to the SM. This is due to the positive interference between the diagram with κ_λ and the other non-resonant contributions. Therefore, as $\kappa_\lambda^{(1)} \gtrsim 1$ in most cases, the di-Higgs cross section in the 2HDM is likely to be enhanced when the one-loop corrected THCs are taken into account. Current projections for measuring deviations in κ_λ via di-Higgs production at e^+e^- colliders give an accuracy of about 10% for the values of $\kappa_\lambda^{(1)}$ found in our paper [39]. This reinforces di-Higgs production as a promising probe of BSM physics, even in the absence of significant deviations in other Higgs-boson couplings. We furthermore found that the two methods of determining $\kappa_\lambda^{(1)}$ (with the effective potential and with a fully diagrammatic approach) yield similar di-Higgs cross section predictions, both absolute and differential, with a relative difference within 1-5%. This confirms the effective potential approach as a good approximation to account for the one-loop corrections to κ_λ in the Zhh cross section.

We also examined the impact of the one-loop corrected THC $\lambda_{hhH}^{(1)}$ on the production cross section. The effect of this coupling enters through a resonant diagram mediated by H, which can potentially produce a resonant peak at $m_{hh} = m_H$. To estimate the potential sensitivity to the $\lambda_{hhH}^{(1)}$ via the H resonance peak we considered the main Higgs decay channel to $b\bar{b}$, giving a final state $Zhh \to Zb\bar{b}b\bar{b}$, incorporating acceptance cuts inspired by e^+e^- experimental analyses and considering b-tagging efficiencies. To model experimental uncertainties, we applied Gaussian smearing to theoretical cross section distributions with smearing values of 0%, 2%, 5%, and 10%, where 5% reflects current expectations for m_{hh} resolution [39, 104]

(which could potentially improve in the future). Additionally, we set bin sizes ensuring at least two events in each bin in the kinematically allowed region ($2m_h < m_{hh} < \sqrt{s} - m_Z$). We quantified the sensitivity to the H resonance peak using a likelihood ratio statistical test, which gives the statistical significance of the H resonance peak against the no-resonance hypothesis, denoted by Z. For all our benchmark points (except for BPal), the significance of the H resonance peak is enhanced when the one-loop corrections to the THCs are considered, since the BPs were chosen such that $\lambda_{hhH}^{(1)} > \lambda_{hhH}^{(0)}$. We found promising significance values for all studied benchmark points. For BP1, BP2, and BPext, we obtained $Z^{(1)} > 10$ even under pessimistic smearing conditions (10%). For BP3 and BPsign, $Z^{(1)} \sim 5$ was achieved in all considered scenarios. These promising results suggest that high-energy e^+e^- colliders could provide a unique opportunity to probe a BSM H boson in the mass range $250 \text{ GeV} \lesssim m_H \lesssim 400 \text{ GeV}$ and its triple coupling to two SM-like Higgs bosons, λ_{hhH}.

Finally, we analyzed the degrading effect that smearing and binning of the cross section distributions have on the sensitivity to the H resonance and hence to $\lambda_{hhH}^{(1)}$. Without smearing (which is an unrealistic scenario), the statistical significance of the H resonance peak is significantly reduced after the binning of the cross section, i.e. compared to the significance values obtained from the differential cross section. However, even for small smearing values of 2%, the degradation of the significance is dominated by the detector resolution to determine m_{hh}, since the subsequent binning has a minimal effect on the significance. For larger smearing values of 5% and 10%, the detector resolution completely dominates the degradation of the H resonance peak, and binning effects become negligible in comparison. We concluded that the primary limiting factor in accessing λ_{hhH} via the H resonance peak is the finite experimental resolution in m_{hh}. These experimental uncertainties, but especially smearing, dilute the resonant peak, making it more difficult to distinguish it from the continuum background. This effect is especially important for narrow resonances. In particular, the sensitivity to the sign of the THC λ_{hhH} is also affected by these experimental uncertainties, as we observed in BPsign. Therefore, at future e^+e^- colliders, a high detector resolution will be crucial to probe H resonances in the di-Higgs channel and thus to access the THC λ_{hhH}.

In summary, our work emphasizes the fact that higher-order corrected THCs can significantly modify the di-Higgs production cross section in BSM Higgs models, and in many cases they can enhance it even when the alignment limit is imposed. Therefore, with this work we emphasize that it is crucial to include these higher-order corrections in any phenomenological analysis of di-Higgs production. Moreover, our study highlights the challenge of accessing the H resonance peak and its associated THC λ_{hhH} at e^+e^- colliders. We provided an estimate of the experimental precision required to achieve this, underlining the importance of high-resolution detectors in future collider experiments.

Acknowledgments

A   Enhancement Factors for Polarized Cross Section

The amplitude of the di-Higgs process $e^+e^- \to Zhh$ can be generically written as

$$\mathcal{M} = \bar{v}\gamma_\mu(g_L P_L + g_R P_R)u X^{\mu\nu}\epsilon_\nu^* \,, \tag{39}$$

where $X^{\mu\nu}$ denotes the part of the diagram attached to the right end of the Z boson propagators in Fig. 1. If one considers initially polarized electron-positron pairs, the polarized amplitudes can be written as

$$\mathcal{M}_{LR} = \bar{v}_R\gamma_\mu\left(g_L P_L + g_R P_R\right)u_L X^{\mu\nu}\epsilon_\nu^* = g_L\bar{v}_R\gamma_\mu P_L u_L X^{\mu\nu}\epsilon_\nu^* \,, \tag{40}$$

$$\mathcal{M}_{RL} = \bar{v}_L\gamma_\mu\left(g_L P_L + g_R P_R\right)u_R X^{\mu\nu}\epsilon_\nu^* = g_R\bar{v}_L\gamma_\mu P_R u_R X^{\mu\nu}\epsilon_\nu^* \,. \tag{41}$$

To compute the unpolarized amplitude squared we have

$$\begin{aligned}|\bar{\mathcal{M}}|^2 &= \frac{1}{4}\sum_{\text{spin}}\mathcal{M} \\ &= \frac{1}{4}\frac{1}{2}\left[\left(g_L^2 + g_R^2\right)\text{tr}(p_1\gamma_\mu p_2\gamma_\alpha) + \left(g_L^2 - g_R^2\right)\text{tr}\left(p_1\gamma_\mu p_2\gamma_\alpha\gamma^5\right)\right]X^{\mu\nu}\left(X^{\alpha\beta}\right)^\dagger\epsilon_\nu^*\epsilon_\beta \,,\end{aligned} \tag{42}$$

where $p_{1,2}$ is the momentum of the positron/electron. Since $X^{\mu\nu}$ is real and $\sum\epsilon_\nu^*\epsilon_\beta$ is symmetric, only the trace without γ^5 contributes to the amplitude squared. This can be seen explicitly in the expression for $X^{\mu\nu}$. For all diagrams one has

$$X^{\mu\nu} \propto g^{\mu\nu} \,, \tag{43}$$

except for the A-mediated ones, where

$$X^{\mu\nu} \propto \left(p_{h_1} - p_A\right)^\mu\left(p_{h_2} + p_A\right)^\nu + \left(p_{h_1} \leftrightarrow p_{h_2}\right) \tag{44}$$

so that the combination $X^{\mu\nu}\left(X^{\alpha\beta}\right)^\dagger\sum_{\text{spin}}\epsilon_\nu^*\epsilon_\beta$ gives a symmetric tensor under the μ and α indices.

In the case of the LR polarized amplitude one has

$$\begin{aligned}\mathcal{M}_{LR} &= \bar{v}_R\gamma_\mu\left(g_L P_L + g_R P_R\right)u_L X^{\mu\nu}\epsilon_\nu^* = g_L\bar{v}_R\gamma_\mu P_L u_L X^{\mu\nu}\epsilon_\nu^* \\ &= g_L\left(\bar{v}_R + \bar{v}_L\right)\gamma_\mu P_L\left(u_L + u_R\right)X^{\mu\nu}\epsilon_\nu^* \,,\end{aligned} \tag{45}$$

where we used the relation of the chiral projectors. To compute the amplitude squared,

$$|\mathcal{M}_{LR}|^2 = \frac{1}{2}g_L^2\left[\text{tr}(p_1\gamma_\mu p_2\gamma_\alpha) + \text{tr}\left(p_1\gamma_\mu p_2\gamma_\alpha\gamma^5\right)\right]X^{\mu\nu}\left(X^{\alpha\beta}\right)^\dagger\epsilon_\nu^*\epsilon_\beta \,, \tag{46}$$

where again only the traces without γ^5 contribute. The result for the RL amplitude is the same but interchanging g_L for g_R. Comparing the expressions for polarized and unpolarized squared amplitudes, one arrives at the expressions in Eq. (21).

B   Results for $\sqrt{s} = 1$ TeV

Here we briefly summarize our results of the sensitivity to $\lambda_{hhH}^{(1)}$ from the double Higgs-strahlung process at an e^+e^- collider operating at a center-of-mass energy of $\sqrt{s} = 1$ TeV. The differential distributions for the BPs defined in Tab. 4 can be found in Figs. 9 to 12, where we use the same notation as in the 500 GeV analysis, see Sect. 5.2. Overall, the obtained values of the total cross sections are smaller than in the $\sqrt{s} = 500$ GeV case, discussed in Sect. 5.2, as expected in the Higgs-strahlung channel.

The effects induced by $\kappa_\lambda^{(1)}$ are very similar to the $\sqrt{s} = 500$ GeV case. For the points where $\kappa_\lambda^{(1)}$ is large (namely BP1, BP2, BPsign and BPext), an enhancement of the non-resonant contributions is found in the differential distributions. More specifically, this cross section enhancement is more important close to the threshold production.

Regarding the sensitivity to $\lambda_{hhH}^{(1)}$, it enters again via the H resonance production. For the considered BPs, we get smaller statistical significances Z from all the H resonances compared to the $\sqrt{s} = 500$ GeV case, except for BP2 and BPsign. The reason for this is that m_H is relatively high, and therefore a larger center-of-mass energy favors the production the H resonance. Similar to the 500 GeV case, the enhancement from $\kappa_\lambda^{(1)}$ implies also more events in the H resonance peak, which could overcome the problem of having a small number of events like in the SM. However, as stated in Sect. 5.2, a complete analysis for an e^+e^- collider at $\sqrt{s} = 1$ TeV should include the WW fusion di-Higgs production, $e^+e^- \to \nu\bar{\nu}\, hh$, which is beyond the scope of this paper.

Smearing and binning of the distributions has similar effects as in the 500 GeV case. Smearing is the limiting experimental effect to detect the H resonance peak, as it can be seen in the values of the statistical significances Z, shown in the Figs. 9 to 13, and also summarized in Tab. 7. Binning is only important when considering unsmeared distributions, which are not realistic from an experimental point of view. When smearing is considered, the posterior binning of the distributions does not have a big effect on the obtained values for Z.

C   Significance of the H Resonance with More Stringent Event Cuts

In this appendix we consider the same selection cuts as applied in Ref. [40]. This study, compared to ours, takes into account further cuts in the event selection to further suppress the $Zhh \to Zb\bar{b}b\bar{b}$ signal versus the SM background. These extra cuts reduce the final detected number of events to 17% of the inclusive theoretical prediction, compared to the $\sim 60\%$ obtained when applying only the preselection cuts as we considered in the analysis in the main text. However, it should be kept in mind that these cuts were optimized for non-resonant di-Higgs production.

The results for the significances for the 500 GeV case are summarized in Tab. 8. Due to the smaller numbers of events that we can reconstruct compared to the previous analysis, now binning plays also a dominant role in the degradation of the obtained values of Z. With these extra cuts, the bin size gets very large compared to the values shown in 6. For the considered points, the bin sizes obtained with these more stringent cuts are over a factor of
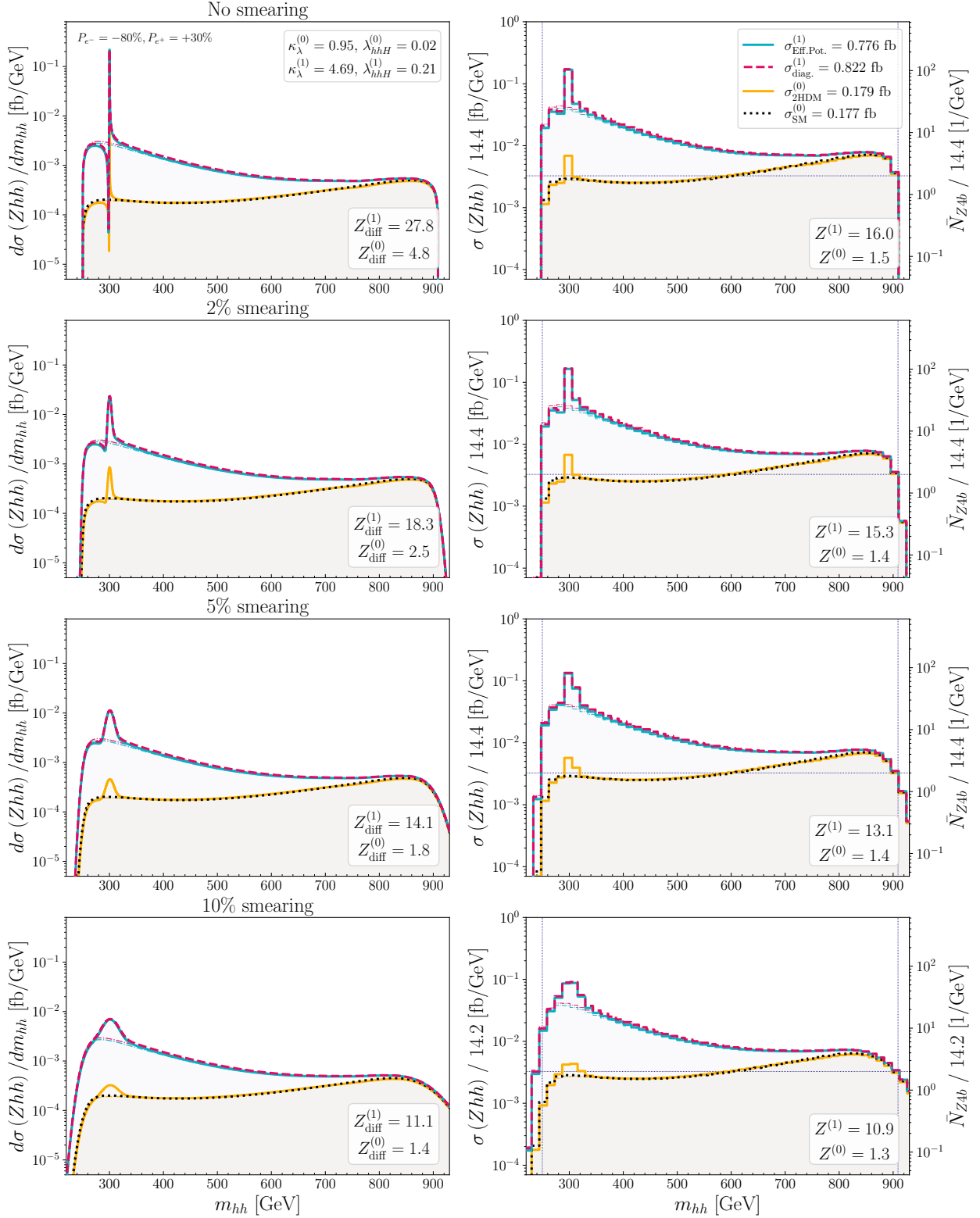
Figure 9: Differential distribution as a function of m_{hh} for BP1 at $\sqrt{s} = 1$ TeV for $P_{e^-} = -80\%$ and $P_{e^+} = +30\%$. The color coding is the same as in Fig. 4.
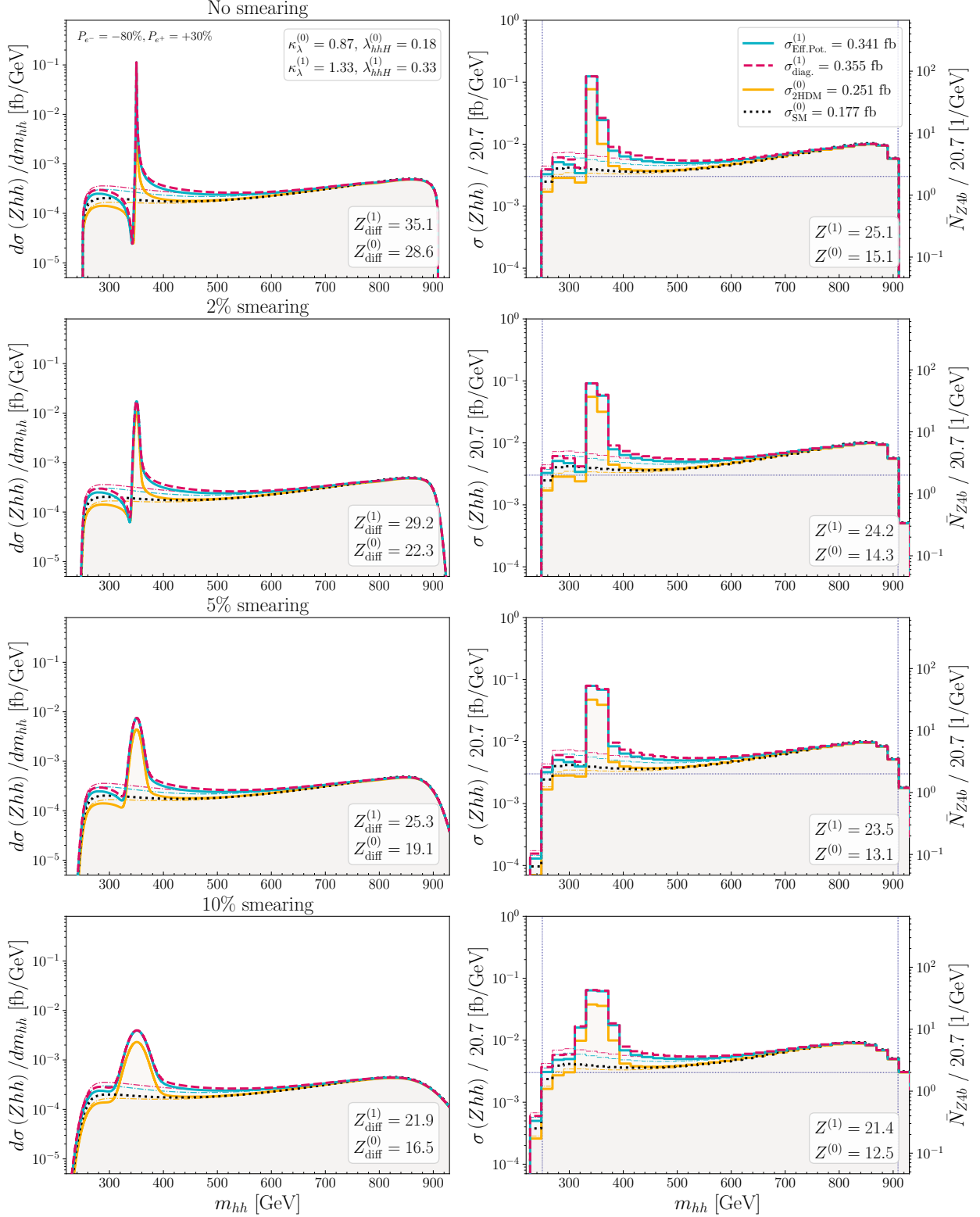
Figure 10: Differential distribution as a function of m_{hh} for BP2 at $\sqrt{s} = 1$ TeV for $P_{e^-} = -80\%$ and $P_{e^+} = +30\%$. The color coding is the same as in Fig. 4.

Figure 11: Differential distribution as a function of m_{hh} for BP3 at $\sqrt{s} = 1$ TeV for $P_{e^-} = -80\%$ and $P_{e^+} = +30\%$. The color coding is the same as in Fig. 4.
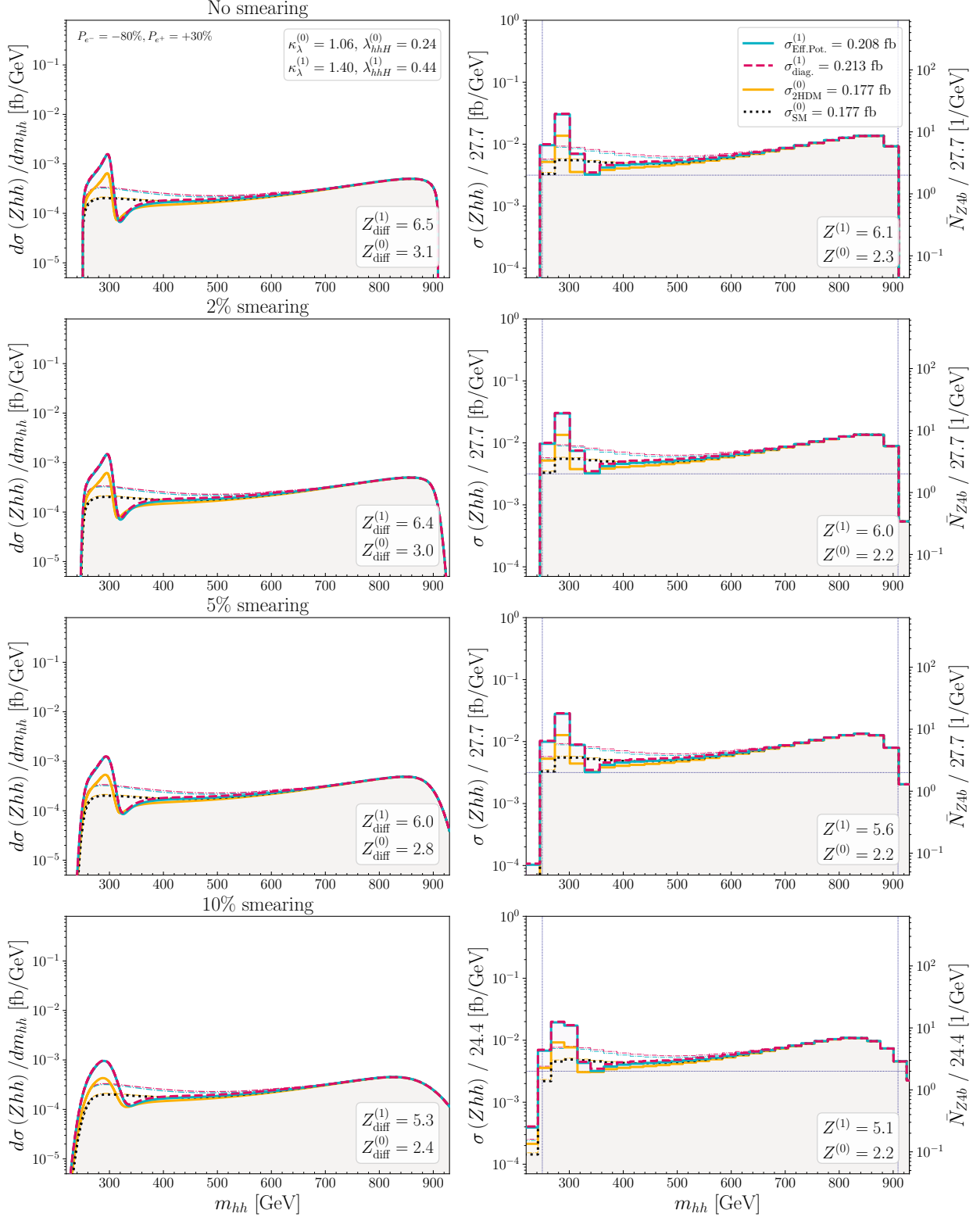
Figure 12: Differential distribution as a function of m_{hh} for BPsign at $\sqrt{s} = 1$ TeV f or $P_{e^-} = -80\%$ and $P_{e^+} = +30\%$. The color coding is the same as in Fig. 4

Figure 13: Differential distribution as a function of m_{hh} for BPext at $\sqrt{s} = 1$ TeV for $P_{e^-} = -80\%$ and $P_{e^+} = +30\%$. The color coding is the same as in Fig. 4.
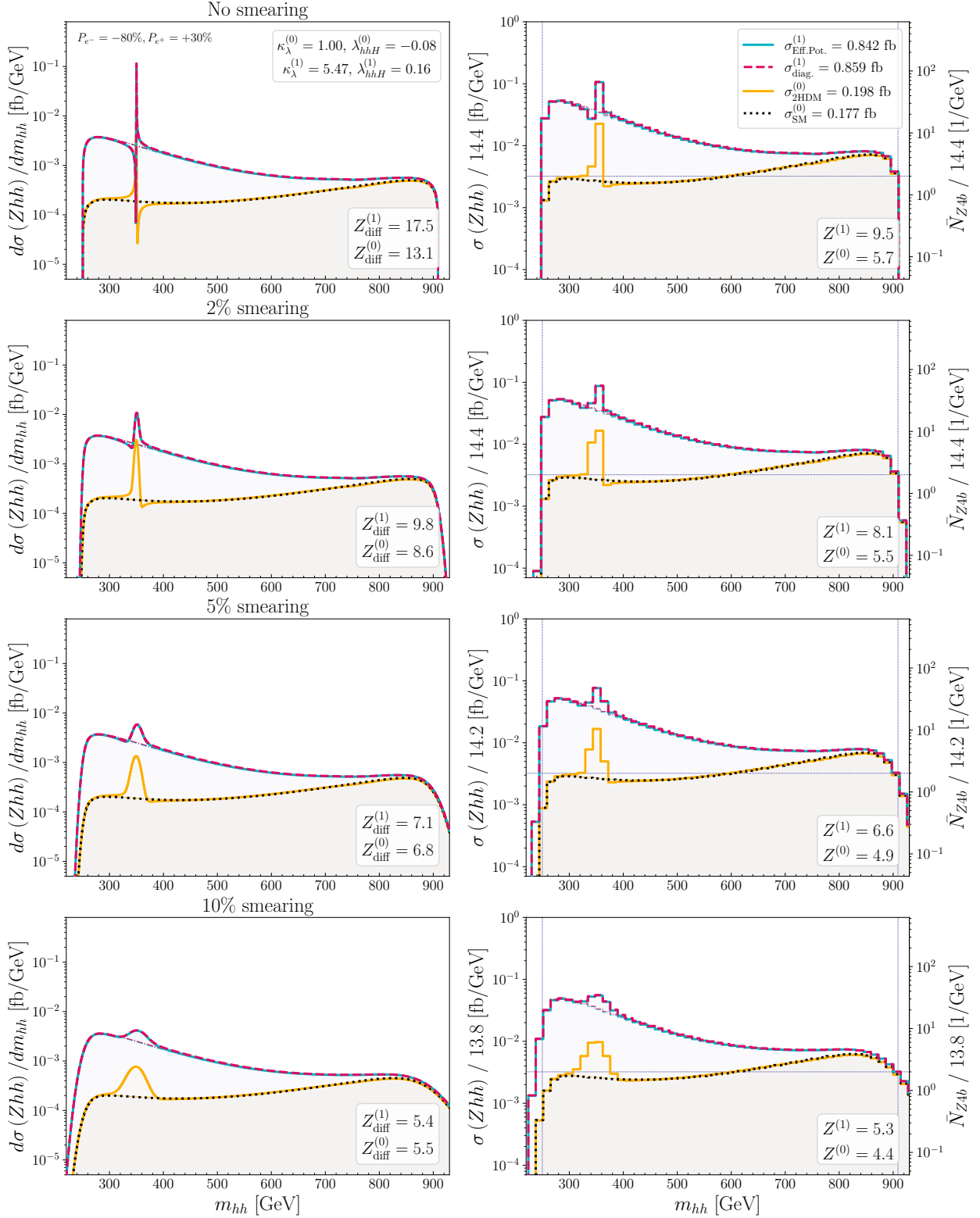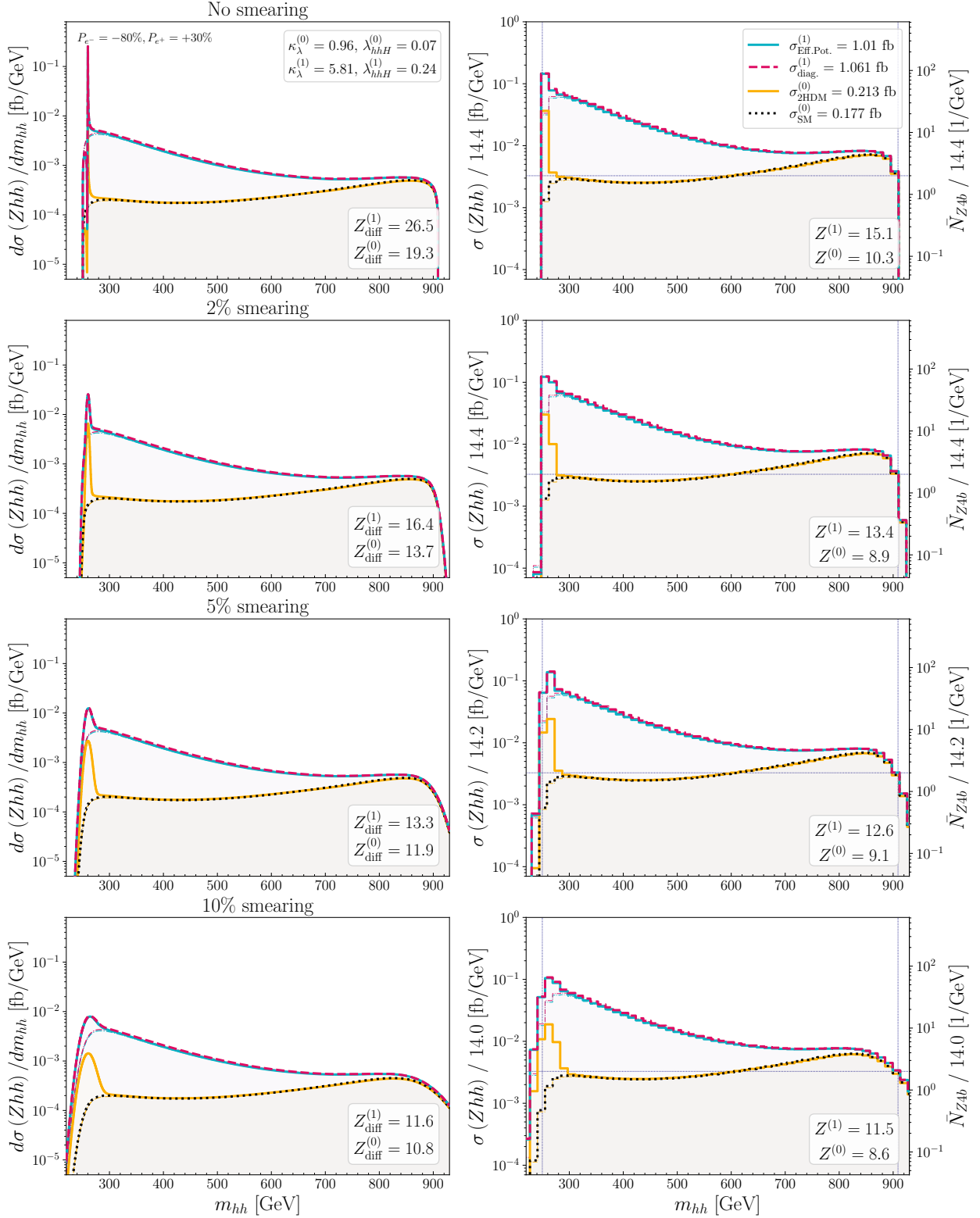
Point	Smearing	$\text{Bin}^{(1)}_{-+}$	$\text{Bin}^{(1)}_{+-}$	$Z^{(1)}_{\text{diff}}$	$Z^{(1)}$	$\text{Bin}^{(0)}_{+-}$	$\text{Bin}^{(0)}_{-+}$	$Z^{(0)}_{\text{diff}}$	$Z^{(0)}$
BP1	0%	14.4	16.2	27.8	16.0	26.6	39.2	4.8	1.5
	2%	14.4	19.8	18.3	15.3	26.6	39.2	2.5	1.4
	5%	14.4	19.8	14.1	13.1	26.6	39.2	1.8	1.4
	10%	14.2	19.4	11.1	10.9	29.5	34.2	1.4	1.3
BP2	0%	20.7	27.8	35.1	25.1	33.8	39.8	28.6	18.6
	2%	20.7	27.8	29.2	24.2	33.6	39.8	22.3	17.9
	5%	20.7	27.8	25.3	23.5	33.6	39.9	19.1	17.0
	10%	20.7	27.9	21.9	21.4	33.7	46.5	16.5	15.6
BP3	0%	27.7	34.5	6.5	6.1	28.6	39.3	3.1	2.3
	2%	27.7	34.5	6.4	6.0	28.6	39.3	3.0	2.3
	5%	27.7	34.5	6.0	5.6	28.5	39.3	2.8	2.2
	10%	24.4	34.6	5.3	5.1	26.6	37.1	2.4	2.3
BPsign	0%	14.4	16.2	17.5	9.5	23.9	33.8	13.1	6.6
	2%	14.4	18.2	9.8	8.1	23.9	33.8	8.6	6.2
	5%	14.2	19.4	7.1	6.6	26.5	33.8	6.8	5.6
	10%	13.8	18.2	5.4	5.3	26.4	33.9	5.5	5.2
BPext	0%	14.4	16.2	26.5	15.1	19.6	28.1	19.3	13.0
	2%	14.4	18.2	16.4	13.4	19.2	27.5	13.7	10.7
	5%	14.2	19.4	13.3	12.6	18.8	27.4	11.9	11.0
	10%	14.0	18.2	11.6	11.5	18.6	27.3	10.8	10.5

Table 7: Statistical significance Z for all the benchmark points (BPs) for a center-of-mass energy of $\sqrt{s} = 1$ TeV. We use the same notation as in Tab. 6.

two larger compared with the analysis presented in the main text. Therefore, as expected, the sensitivity to λ_{hhH} would worsen with these more stringent cuts. However, it should be noted that even with this low number of events, after considering the one-loop corrections to λ_{hhH} the values for the significance Z are above 5 for the points BP1, BP2 and BPext for smearing values smaller or equal to 5%. This emphasizes again the relevance that one-loop corrections can have in a phenomenological analysis of the Zhh signal in BSM models.

References

[1] G. Aad *et al.*, "Observation of a new particle in the search for the Standard Model Higgs boson with the ATLAS detector at the LHC," *Phys. Lett. B*, vol. 716, pp. 1–29, 2012. arXiv: 1207.7214 [hep-ex].

[2] S. Chatrchyan *et al.*, "Observation of a New Boson at a Mass of 125 GeV with the CMS Experiment at the LHC," *Phys. Lett. B*, vol. 716, pp. 30–61, 2012. arXiv: 1207.7235 [hep-ex].

Point	Smearing	$\mathrm{Bin}^{(1)}_{-+}$	$\mathrm{Bin}^{(1)}_{+-}$	$Z^{(1)}_{\mathrm{diff}}$	$Z^{(1)}$	$\mathrm{Bin}^{(0)}_{+-}$	$\mathrm{Bin}^{(0)}_{-+}$	$Z^{(0)}_{\mathrm{diff}}$	$Z^{(0)}$
BP1	0%	15.1	18.6	14.8	7.8	26.6	39.9	2.2	0.5
	2%	15.1	18.6	9.2	7.0	26.6	39.9	0.9	0.4
	5%	14.0	18.6	6.8	6.2	26.6	39.9	0.6	0.4
	10%	13.1	18.6	5.3	5.1	26.6	39.9	0.4	0.4
BP2	0%	22.8	35.3	12.2	7.6	26.6	39.9	9.7	4.5
	2%	22.8	35.3	9.0	7.4	26.6	39.9	6.4	4.4
	5%	22.8	35.3	7.2	6.5	26.6	39.9	4.9	4.2
	10%	22.8	35.2	5.7	5.5	26.6	39.9	3.9	3.7
BP3	0%	22.8	34.7	3.1	2.7	26.6	33.3	1.5	1.4
	2%	27.6	34.7	3.0	2.9	26.6	33.3	1.5	1.3
	5%	27.6	34.7	2.8	2.7	26.6	33.3	1.4	1.3
	10%	27.6	34.7	2.4	2.4	26.6	39.9	1.1	1.1
BPsign	0%	12.3	16.3	6.9	3.4	26.6	33.6	4.5	1.5
	2%	12.3	16.3	3.4	2.9	26.6	33.6	2.2	1.5
	5%	12.7	16.3	2.3	2.2	26.6	33.6	1.6	1.3
	10%	12.3	15.7	1.7	1.7	26.6	39.9	1.2	1.1
BPext	0%	12.3	16.3	16.7	9.1	23.5	28.5	11.5	6.5
	2%	12.3	16.3	10.1	8.3	23.5	28.5	7.4	6.5
	5%	12.3	16.3	8.0	7.6	23.5	33.3	6.2	5.9
	10%	11.6	15.7	7.0	6.9	25.0	33.3	5.5	5.2

Table 8: Statistical significance Z for all the benchmark points (BPs) for a center-of-mass energy of $\sqrt{s} = 500$ GeV. Here we consider that only 17% of the theoretically calculated $Zb\bar{b}b\bar{b}$ events enter our evaluation. This corresponds to the result of Ref. [40] to suppress the signal versus background in the Zhh channel. We use the same notation as in Tab. 6.

[3]   G. Aad *et al.*, "A detailed map of Higgs boson interactions by the ATLAS experiment ten years after the discovery," *Nature*, vol. 607, no. 7917, pp. 52–59, 2022, [Erratum: Nature 612, E24 (2022)]. arXiv: 2207.00092 [hep-ex].

[4]   A. Tumasyan *et al.*, "A portrait of the Higgs boson by the CMS experiment ten years after the discovery.," *Nature*, vol. 607, no. 7917, pp. 60–68, 2022, [Erratum: Nature 623, (2023)]. arXiv: 2207.00043 [hep-ex].

[5]   G. Aad *et al.*, "Combination of Searches for Higgs Boson Pair Production in pp Collisions at s=13 TeV with the ATLAS Detector," *Phys. Rev. Lett.*, vol. 133, no. 10, p. 101 801, 2024. arXiv: 2406.09971 [hep-ex].

[6]   A. Hayrapetyan *et al.*, "Constraints on the Higgs boson self-coupling from the combination of single and double Higgs boson production in proton-proton collisions at s=13TeV," *Phys. Lett. B*, vol. 861, p. 139 210, 2025. arXiv: 2407.13554 [hep-ex].

Point	Smearing	$\text{Bin}^{(1)}_{-+}$	$\text{Bin}^{(1)}_{+-}$	$Z^{(1)}_{\text{diff}}$	$Z^{(1)}$	$\text{Bin}^{(0)}_{+-}$	$\text{Bin}^{(0)}_{-+}$	$Z^{(0)}_{\text{diff}}$	$Z^{(0)}$
BP1	0%	29.5	40.0	15.5	7.0	75.0	102.5	2.7	0.7
	2%	30.5	40.0	10.2	6.0	75.0	102.5	1.4	0.7
	5%	34.0	46.1	7.8	5.6	75.0	102.5	1.0	0.6
	10%	35.3	48.6	6.2	5.7	73.1	103.0	0.8	0.6
BP2	0%	52.4	89.1	18.9	10.6	112.4	113.2	15.4	7.5
	2%	52.4	89.2	15.7	10.4	112.4	112.4	12.0	6.9
	5%	52.4	89.3	13.6	10.5	107.3	112.4	10.3	7.2
	10%	52.7	68.2	11.8	10.6	77.7	106.2	8.9	7.8
BP3	0%	78.2	109.1	3.4	1.7	92.8	114.1	1.6	0.8
	2%	78.2	109.1	3.3	1.7	92.8	114.2	1.6	0.8
	5%	78.2	108.8	3.1	1.7	92.6	114.2	1.5	0.8
	10%	75.2	108.1	2.8	1.8	92.4	114.2	1.3	0.8
BPsign	0%	29.5	38.3	9.7	4.3	75.0	106.7	7.2	2.6
	2%	29.5	40.0	5.4	3.1	75.0	106.7	4.7	2.6
	5%	32.7	46.1	3.9	2.5	75.0	106.5	3.7	2.6
	10%	35.3	46.1	3.0	2.5	75.0	105.0	3.0	2.5
BPext	0%	29.5	40.0	14.8	8.0	64.3	89.9	10.8	6.5
	2%	29.5	40.0	9.2	6.9	64.3	89.9	7.6	6.5
	5%	32.7	46.1	7.4	6.2	61.7	89.9	6.7	5.4
	10%	35.3	46.1	6.5	6.2	60.9	86.0	6.0	5.3

Table 9: Statistical significance Z for all the benchmark points (BPs) for a center-of-mass energy of $\sqrt{s} = 1$ TeV. Here we consider that only 17% of the theoretically calculated $Zb\bar{b}b\bar{b}$ events enter our evaluation. This corresponds to the result of Ref. [40] to suppress the signal versus background in the Zhh channel. We use the same notation as in Tab. 6.

[7] T. D. Lee, "A Theory of Spontaneous T Violation," *Phys. Rev. D*, vol. 8, G. Feinberg, Ed., pp. 1226–1239, 1973.

[8] J. F. Gunion, H. E. Haber, G. L. Kane, and S. Dawson, *The Higgs Hunter's Guide*. 2000, vol. 80.

[9] M. Aoki, S. Kanemura, K. Tsumura, and K. Yagyu, "Models of Yukawa interaction in the two Higgs doublet model, and their collider phenomenology," *Phys. Rev. D*, vol. 80, p. 015 017, 2009. arXiv: 0902.4665 [hep-ph].

[10] G. C. Branco, P. M. Ferreira, L. Lavoura, M. N. Rebelo, M. Sher, and J. P. Silva, "Theory and phenomenology of two-Higgs-doublet models," *Phys. Rept.*, vol. 516, pp. 1–102, 2012. arXiv: 1106.0034 [hep-ph].

[11] J. Bernon, J. F. Gunion, H. E. Haber, Y. Jiang, and S. Kraml, "Scrutinizing the alignment limit in two-Higgs-doublet models: m_h=125 GeV," *Phys. Rev. D*, vol. 92, no. 7, p. 075 004, 2015. arXiv: 1507.00933 [hep-ph].

[12] F. Arco, S. Heinemeyer, and M. J. Herrero, "Exploring sizable triple Higgs couplings in the 2HDM," *Eur. Phys. J. C*, vol. 80, no. 9, p. 884, 2020. arXiv: 2005.10576 [hep-ph].

[13] H. Abouabid *et al.*, "Benchmarking di-Higgs production in various extended Higgs sector models," *JHEP*, vol. 09, p. 011, 2022. arXiv: 2112.12515 [hep-ph].

[14] F. Arco, S. Heinemeyer, and M. J. Herrero, "Triple Higgs couplings in the 2HDM: the complete picture," *Eur. Phys. J. C*, vol. 82, no. 6, p. 536, 2022. arXiv: 2203.12684 [hep-ph].

[15] S. Kanemura, S. Kiyoura, Y. Okada, E. Senaha, and C. P. Yuan, "New physics effect on the Higgs selfcoupling," *Phys. Lett. B*, vol. 558, pp. 157–164, 2003. arXiv: hep-ph/0211308.

[16] S. Kanemura, Y. Okada, E. Senaha, and C. .-. Yuan, "Higgs coupling constants as a probe of new physics," *Phys. Rev. D*, vol. 70, p. 115 002, 2004. arXiv: hep-ph/0408364.

[17] H. Bahl, J. Braathen, M. Gabelmann, and G. Weiglein, "anyH3: precise predictions for the trilinear Higgs coupling in the Standard Model and beyond," *Eur. Phys. J. C*, vol. 83, no. 12, p. 1156, 2023. arXiv: 2305.03015 [hep-ph].

[18] J. Braathen and S. Kanemura, "On two-loop corrections to the Higgs trilinear coupling in models with extended scalar sectors," *Phys. Lett. B*, vol. 796, pp. 38–46, 2019. arXiv: 1903.05417 [hep-ph].

[19] J. Braathen and S. Kanemura, "Leading two-loop corrections to the Higgs boson self-couplings in models with extended scalar sectors," *Eur. Phys. J. C*, vol. 80, no. 3, p. 227, 2020. arXiv: 1911.11507 [hep-ph].

[20] H. Bahl, J. Braathen, and G. Weiglein, "New Constraints on Extended Higgs Sectors from the Trilinear Higgs Coupling," *Phys. Rev. Lett.*, vol. 129, no. 23, p. 231 802, 2022. arXiv: 2202.03453 [hep-ph].

[21] M. Aoki, S. Kanemura, M. Kikuchi, and K. Yagyu, "Radiative corrections to the Higgs boson couplings in the triplet model," *Phys. Rev. D*, vol. 87, no. 1, p. 015 012, 2013. arXiv: 1211.6029 [hep-ph].

[22] A. Arhrib, R. Benbrik, J. El Falaki, and A. Jueid, "Radiative corrections to the Triple Higgs Coupling in the Inert Higgs Doublet Model," *JHEP*, vol. 12, p. 007, 2015. arXiv: 1507.03630 [hep-ph].

[23] S. Kanemura, M. Kikuchi, and K. Yagyu, "One-loop corrections to the Higgs self-couplings in the singlet extension," *Nucl. Phys. B*, vol. 917, pp. 154–177, 2017. arXiv: 1608.01582 [hep-ph].

[24] C.-W. Chiang, A.-L. Kuo, and K. Yagyu, "One-loop renormalized Higgs boson vertices in the Georgi-Machacek model," *Phys. Rev. D*, vol. 98, no. 1, p. 013 008, 2018. arXiv: 1804.02633 [hep-ph].

[25] P. Basler, M. Mühlleitner, and J. Wittbrodt, "The CP-Violating 2HDM in Light of a Strong First Order Electroweak Phase Transition and Implications for Higgs Pair Production," *JHEP*, vol. 03, p. 061, 2018. arXiv: 1711.04097 [hep-ph].

[26] T. Biekötter, S. Heinemeyer, J. M. No, M. O. Olea-Romacho, and G. Weiglein, "The trap in the early Universe: impact on the interplay between gravitational waves and LHC physics in the 2HDM," *JCAP*, vol. 03, p. 031, 2023. arXiv: 2208.14466 [hep-ph].

[27] J. de Blas *et al.*, "Higgs Boson Studies at Future Particle Colliders," *JHEP*, vol. 01, p. 139, 2020. arXiv: 1905.03764 [hep-ph].

[28] J. Alison *et al.*, "Higgs boson potential at colliders: Status and perspectives," *Rev. Phys.*, vol. 5, B. Di Micco, M. Gouzevitch, J. Mazzitelli, and C. Vernieri, Eds., p. 100045, 2020. arXiv: 1910.00012 [hep-ph].

[29] V. A. Ilyin, A. E. Pukhov, Y. Kurihara, Y. Shimizu, and T. Kaneko, "Probing the H^3 vertex in e+ e-, gamma e and gamma gamma collisions for light and intermediate Higgs bosons," *Phys. Rev. D*, vol. 54, pp. 6717–6727, 1996. arXiv: hep-ph/9506326.

[30] P. Osland and P. N. Pandita, "Measuring the trilinear couplings of MSSM neutral Higgs bosons at high-energy e+ e- colliders," *Phys. Rev. D*, vol. 59, p. 055013, 1999. arXiv: hep-ph/9806351.

[31] A. Djouadi, W. Kilian, M. Mühlleitner, and P. M. Zerwas, "Testing Higgs selfcouplings at e+ e- linear colliders," *Eur. Phys. J. C*, vol. 10, pp. 27–43, 1999. arXiv: hep-ph/9903229.

[32] M. M. Mühlleitner, "Higgs particles in the standard model and supersymmetric theories," Ph.D. dissertation, Hamburg U., 2000. arXiv: hep-ph/0008127.

[33] A. Arbey *et al.*, "Physics at the e+ e- Linear Collider," *Eur. Phys. J. C*, vol. 75, no. 8, G. Moortgat-Pick *et al.*, Eds., p. 371, 2015. arXiv: 1504.01726 [hep-ph].

[34] T. K. Charles *et al.*, "The Compact Linear Collider (CLIC) - 2018 Summary Report," vol. 2/2018, P. N. Burrows *et al.*, Eds., Dec. 2018. arXiv: 1812.06018 [physics.acc-ph].

[35] F. Arco, S. Heinemeyer, and M. J. Herrero, "Sensitivity to triple Higgs couplings via di-Higgs production in the 2HDM at e^+e^- colliders," *Eur. Phys. J. C*, vol. 81, no. 10, p. 913, 2021. arXiv: 2106.11105 [hep-ph].

[36] P. Bambade *et al.*, "The International Linear Collider: A Global Project," Mar. 2019. arXiv: 1903.01629 [hep-ex].

[37] M. Bai *et al.*, "C³: A "Cool" Route to the Higgs Boson and Beyond," in *Snowmass 2021*, Oct. 2021. arXiv: 2110.15800 [hep-ex].

[38] C. Balazs *et al.*, "The Linear Collider Facility (LCF) at CERN," Mar. 2025. arXiv: 2503.24049 [hep-ex].

[39] C. Balazs *et al.*, "A Linear Collider Vision for the Future of Particle Physics," Mar. 2025. arXiv: 2503.19983 [hep-ex].

[40] C. F. Dürig, "Measuring the Higgs Self-coupling at the International Linear Collider," Ph.D. dissertation, Hamburg U., Hamburg, 2016. [Online]. Available: https://bib-pubdb1.desy.de/record/310520.

[41] H. Abramowicz *et al.*, "Higgs physics at the CLIC electron–positron linear collider," *Eur. Phys. J. C*, vol. 77, no. 7, p. 475, 2017. arXiv: 1608.07538 [hep-ex].

[42] P. Roloff, U. Schnoor, R. Simoniello, and B. Xu, "Double Higgs boson production and Higgs self-coupling extraction at CLIC," *Eur. Phys. J. C*, vol. 80, no. 11, p. 1010, 2020. arXiv: 1901.05897 [hep-ex].

[43] J. M. Torndal and J. List, "Higgs self-coupling measurement at the International Linear Collider," in *International Workshop on Future Linear Colliders*, Jul. 2023. arXiv: 2307.16515 [hep-ph].

[44] J. M. Torndal, J. List, D. Ntounis, and C. Vernieri, "Higgs self-coupling measurement at future e^+e^- colliders," *PoS*, vol. EPS-HEP2023, p. 406, 2024. arXiv: 2311.16774 [hep-ex].

[45] ATLAS and CMS Collaborations, "Highlights of the HL-LHC physics projections by ATLAS and CMS," Apr. 2025. arXiv: 2504.00672 [hep-ex].

[46] A. Abada *et al.*, "FCC-ee: The Lepton Collider: Future Circular Collider Conceptual Design Report Volume 2," *Eur. Phys. J. ST*, vol. 228, no. 2, pp. 261–623, 2019.

[47] M. Dong *et al.*, "CEPC Conceptual Design Report: Volume 2 - Physics & Detector," J. B. Guimarães da Costa *et al.*, Eds., Nov. 2018. arXiv: 1811.10545 [hep-ex].

[48] W. Abdallah *et al.*, "CEPC Technical Design Report: Accelerator," *Radiat. Detect. Technol. Methods*, vol. 8, no. 1, pp. 1–1105, 2024. arXiv: 2312.14363 [physics.acc-ph].

[49] T. Barklow *et al.*, "ILC Operating Scenarios," Jun. 2015. arXiv: 1506.07830 [hep-ex].

[50] A. Arhrib, R. Benbrik, and C.-W. Chiang, "Probing triple Higgs couplings of the Two Higgs Doublet Model at Linear Collider," *Phys. Rev. D*, vol. 77, p. 115 013, 2008. arXiv: 0802.0319 [hep-ph].

[51] D. Lopez-Val and J. Sola, "Neutral Higgs-pair production at Linear Colliders within the general 2HDM: Quantum effects and triple Higgs boson self-interactions," *Phys. Rev. D*, vol. 81, p. 033 003, 2010. arXiv: 0908.2898 [hep-ph].

[52] E. Asakawa, D. Harada, S. Kanemura, Y. Okada, and K. Tsumura, "Higgs boson pair production in new physics models at hadron, lepton, and photon colliders," *Phys. Rev. D*, vol. 82, p. 115 002, 2010. arXiv: 1009.4670 [hep-ph].

[53] T. Kon, T. Nagura, T. Ueda, and K. Yagyu, "Double Higgs boson production at e^+e^- colliders in the two-Higgs-doublet model," *Phys. Rev. D*, vol. 99, no. 9, p. 095 027, 2019. arXiv: 1812.09843 [hep-ph].

[54] N. Sonmez, "Measuring the triple Higgs self-couplings in two Higgs doublet model," *JHEP*, vol. 10, p. 083, 2018. arXiv: 1806.08963 [hep-ph].

[55] I. Ahmed, U. Nawaz, T. Khurshid, and S. F. Qazi, "Probing Triple Higgs Self-Coupling and Effect of Beam Polarization in Lepton Colliders," *Adv. High Energy Phys.*, vol. 2022, p. 9 735 729, 2022. arXiv: 2110.03920 [hep-ph].

[56] S. R. Coleman and E. J. Weinberg, "Radiative Corrections as the Origin of Spontaneous Symmetry Breaking," *Phys. Rev. D*, vol. 7, pp. 1888–1910, 1973.

[57] E. J. Weinberg, "Radiative corrections as the origin of spontaneous symmetry breaking," Ph.D. dissertation, Harvard U., 1973. arXiv: hep-th/0507214.

[58] P. Basler and M. Mühlleitner, "BSMPT (Beyond the Standard Model Phase Transitions): A tool for the electroweak phase transition in extended Higgs sectors," *Comput. Phys. Commun.*, vol. 237, pp. 62–85, 2019. arXiv: 1803.02846 [hep-ph].

[59] P. Basler, M. Mühlleitner, and J. Müller, "BSMPT v2 a tool for the electroweak phase transition and the baryon asymmetry of the universe in extended Higgs Sectors," *Comput. Phys. Commun.*, vol. 269, p. 108 124, 2021. arXiv: 2007.01725 [hep-ph].

[60] P. Basler, L. Biermann, M. Mühlleitner, J. Müller, R. Santos, and J. Viana, "BSMPT v3 A Tool for Phase Transitions and Primordial Gravitational Waves in Extended Higgs Sectors," Apr. 2024. arXiv: 2404.19037 [hep-ph].

[61] S. Heinemeyer, M. Mühlleitner, K. Radchenko, and G. Weiglein, "Higgs pair production in the 2HDM: impact of loop corrections to the trilinear Higgs couplings and interference effects on experimental limits," *Eur. Phys. J. C*, vol. 85, no. 4, p. 437, 2025. arXiv: 2403.14776 [hep-ph].

[62] S. Heinemeyer, M. Mühlleitner, K. Radchenko, and G. Weiglein, "Higgs Pair Production and Triple Higgs Couplings at the LHC in the 2HDM framework," *PoS*, vol. EPS-HEP2023, p. 411, 2024.

[63] G. Cowan, K. Cranmer, E. Gross, and O. Vitells, "Asymptotic formulae for likelihood-based tests of new physics," *Eur. Phys. J. C*, vol. 71, p. 1554, 2011, [Erratum: Eur.Phys.J.C 73, 2501 (2013)]. arXiv: 1007.1727 [physics.data-an].

[64] S. L. Glashow and S. Weinberg, "Natural Conservation Laws for Neutral Currents," *Phys. Rev. D*, vol. 15, p. 1958, 1977.

[65] E. A. Paschos, "Diagonal Neutral Currents," *Phys. Rev. D*, vol. 15, p. 1966, 1977.

[66] J. F. Gunion and H. E. Haber, "The CP conserving two Higgs doublet model: The Approach to the decoupling limit," *Phys. Rev. D*, vol. 67, p. 075 019, 2003. arXiv: hep-ph/0207010.

[67] R. L. Workman *et al.*, "Review of Particle Physics," *PTEP*, vol. 2022, p. 083C01, 2022.

[68] F. Arco, "Searching for Triple Higgs Couplings: a phenomenological analysis in the Two Higgs Doublet Model," Ph.D. dissertation, Madrid, Autonoma U., 2023. [Online]. Available: http://hdl.handle.net/10486/712636.

[69] R. Coimbra, M. O. P. Sampaio, and R. Santos, "ScannerS: Constraining the phase diagram of a complex scalar singlet at the LHC," *Eur. Phys. J. C*, vol. 73, p. 2428, 2013. arXiv: 1301.2599 [hep-ph].

[70] M. Mühlleitner, M. O. P. Sampaio, R. Santos, and J. Wittbrodt, "ScannerS: parameter scans in extended scalar sectors," *Eur. Phys. J. C*, vol. 82, no. 3, p. 198, 2022. arXiv: 2007.02985 [hep-ph].

[71] S. Bertolini, "Quantum Effects in a Two Higgs Doublet Model of the Electroweak Interactions," *Nucl. Phys. B*, vol. 272, pp. 77–98, 1986.

[72] A. G. Akeroyd, A. Arhrib, and E.-M. Naimi, "Note on tree level unitarity in the general two Higgs doublet model," *Phys. Lett. B*, vol. 490, pp. 119–124, 2000. arXiv: hep-ph/0006035.

[73] I. F. Ginzburg and I. P. Ivanov, "Tree-level unitarity constraints in the most general 2HDM," *Phys. Rev. D*, vol. 72, p. 115 010, 2005. arXiv: hep-ph/0508020.

[74] N. G. Deshpande and E. Ma, "Pattern of Symmetry Breaking with Two Higgs Doublets," *Phys. Rev. D*, vol. 18, p. 2574, 1978.

[75] A. Barroso, P. M. Ferreira, I. P. Ivanov, and R. Santos, "Metastability bounds on the two Higgs doublet model," *JHEP*, vol. 06, p. 045, 2013. arXiv: 1303.5098 [hep-ph].

[76] P. Bechtle, O. Brein, S. Heinemeyer, G. Weiglein, and K. E. Williams, "HiggsBounds: Confronting Arbitrary Higgs Sectors with Exclusion Bounds from LEP and the Tevatron," *Comput. Phys. Commun.*, vol. 181, pp. 138–167, 2010. arXiv: 0811.4169 [hep-ph].

[77] P. Bechtle, O. Brein, S. Heinemeyer, G. Weiglein, and K. E. Williams, "HiggsBounds 2.0.0: Confronting Neutral and Charged Higgs Sector Predictions with Exclusion Bounds from LEP and the Tevatron," *Comput. Phys. Commun.*, vol. 182, pp. 2605–2631, 2011. arXiv: 1102.1898 [hep-ph].

[78] P. Bechtle *et al.*, "HiggsBounds − 4: Improved Tests of Extended Higgs Sectors against Exclusion Bounds from LEP, the Tevatron and the LHC," *Eur. Phys. J. C*, vol. 74, no. 3, p. 2693, 2014. arXiv: 1311.0055 [hep-ph].

[79] P. Bechtle, S. Heinemeyer, O. Stal, T. Stefaniak, and G. Weiglein, "Applying Exclusion Likelihoods from LHC Searches to Extended Higgs Sectors," *Eur. Phys. J. C*, vol. 75, no. 9, p. 421, 2015. arXiv: 1507.06706 [hep-ph].

[80] P. Bechtle *et al.*, "HiggsBounds-5: Testing Higgs Sectors in the LHC 13 TeV Era," *Eur. Phys. J. C*, vol. 80, no. 12, p. 1211, 2020. arXiv: 2006.06007 [hep-ph].

[81] H. Bahl *et al.*, "HiggsTools: BSM scalar phenomenology with new versions of HiggsBounds and HiggsSignals," *Comput. Phys. Commun.*, vol. 291, p. 108 803, 2023. arXiv: 2210.09332 [hep-ph].

[82] P. Bechtle, S. Heinemeyer, O. Stål, T. Stefaniak, and G. Weiglein, "*HiggsSignals*: Confronting arbitrary Higgs sectors with measurements at the Tevatron and the LHC," *Eur. Phys. J. C*, vol. 74, no. 2, p. 2711, 2014. arXiv: 1305.1933 [hep-ph].

[83] P. Bechtle, S. Heinemeyer, O. Stål, T. Stefaniak, and G. Weiglein, "Probing the Standard Model with Higgs signal rates from the Tevatron, the LHC and a future ILC," *JHEP*, vol. 11, p. 039, 2014. arXiv: 1403.1582 [hep-ph].

[84] P. Bechtle, S. Heinemeyer, T. Klingl, T. Stefaniak, G. Weiglein, and J. Wittbrodt, "HiggsSignals-2: Probing new physics with precision Higgs measurements in the LHC 13 TeV era," *Eur. Phys. J. C*, vol. 81, no. 2, p. 145, 2021. arXiv: 2012.09197 [hep-ph].

[85] A. Djouadi, J. Kalinowski, and M. Spira, "HDECAY: A Program for Higgs boson decays in the standard model and its supersymmetric extension," *Comput. Phys. Commun.*, vol. 108, pp. 56–74, 1998. arXiv: hep-ph/9704448.

[86] A. Djouadi, J. Kalinowski, M. Mühlleitner, and M. Spira, "HDECAY: Twenty$_{++}$ years after," *Comput. Phys. Commun.*, vol. 238, pp. 214–231, 2019. arXiv: 1801.09506 [hep-ph].

[87] J. Haller, A. Hoecker, R. Kogler, K. Mönig, T. Peiffer, and J. Stelzer, "Update of the global electroweak fit and constraints on two-Higgs-doublet models," *Eur. Phys. J. C*, vol. 78, no. 8, p. 675, 2018. arXiv: 1803.01853 [hep-ph].

[88] T. Hermann, M. Misiak, and M. Steinhauser, "$\bar{B} \to X_s\gamma$ in the Two Higgs Doublet Model up to Next-to-Next-to-Leading Order in QCD," *JHEP*, vol. 11, p. 036, 2012. arXiv: 1208.2788 [hep-ph].

[89] M. Misiak *et al.*, "Updated NNLO QCD predictions for the weak radiative B-meson decays," *Phys. Rev. Lett.*, vol. 114, no. 22, p. 221 801, 2015. arXiv: 1503.01789 [hep-ph].

[90] M. Misiak and M. Steinhauser, "Weak radiative decays of the B meson and bounds on $M_{H^\pm}$ in the Two-Higgs-Doublet Model," *Eur. Phys. J. C*, vol. 77, no. 3, p. 201, 2017. arXiv: 1702.04571 [hep-ph].

[91] M. Misiak, A. Rehman, and M. Steinhauser, "Towards $\overline{B} \to X_s\gamma$ at the NNLO in QCD without interpolation in m$_c$," *JHEP*, vol. 06, p. 175, 2020. arXiv: 2002.01548 [hep-ph].

[92] J. Ellis, "TikZ-Feynman: Feynman diagrams with TikZ," *Comput. Phys. Commun.*, vol. 210, pp. 103–123, 2017. arXiv: 1601.05437 [hep-ph].

[93] S. Di Vita *et al.*, "A global view on the Higgs self-coupling at lepton colliders," *JHEP*, vol. 02, p. 178, 2018. arXiv: 1711.03978 [hep-ph].

[94] G. Moortgat-Pick *et al.*, "The Role of polarized positrons and electrons in revealing fundamental interactions at the linear collider," *Phys. Rept.*, vol. 460, pp. 131–243, 2008. arXiv: hep-ph/0507011.

[95] J. Tian, "Study of Higgs self-coupling at the ILC based on the full detector simulation at $\sqrt{s} = 500$ GeV and $\sqrt{s} = 1$ TeV," in *3rd Linear Collider Forum*, Hamburg: DESY, 2013, pp. 224–247.

[96] M. A. Thomson, "Particle Flow Calorimetry and the PandoraPFA Algorithm," *Nucl. Instrum. Meth. A*, vol. 611, pp. 25–40, 2009. arXiv: 0907.3577 [physics.ins-det].

[97] S. Catani, Y. L. Dokshitzer, M. Olsson, G. Turnock, and B. R. Webber, "New clustering algorithm for multi - jet cross-sections in e+ e- annihilation," *Phys. Lett. B*, vol. 269, pp. 432–438, 1991.

[98] C. Dürig, K. Fujii, J. List, and J. Tian, "Model Independent Determination of *HWW* coupling and Higgs total width at ILC," in *International Workshop on Future Linear Colliders*, Mar. 2014. arXiv: 1403.7734 [hep-ex].

[99] J. Tian, K. Fujii, and Y. Gao, "Study of Higgs Self-coupling at ILC," Aug. 2010. arXiv: 1008.0921 [hep-ex].

[100] R. Yonamine, K. Ikematsu, S. Uozumi, and K. Fujii, "A Study of top-quark Yukawa coupling measurement in $e^+e^- - > t\bar{t}H$ at sqrt(s) = 500 GeV," Aug. 2010. arXiv: 1008.1110 [hep-ex].

[101] J. Alwall *et al.*, "The automated computation of tree-level and next-to-leading order differential cross sections, and their matching to parton shower simulations," *JHEP*, vol. 07, p. 079, 2014. arXiv: 1405.0301 [hep-ph].

[102] J. Munch Torndal, "ILC capabilities for the measurement of double Higgs production at 500 GeV," in *IDT-WG3-Phys Open Meeting*, 2023. [Online]. Available: https://agenda.linearcollider.org/event/9881/contributions/51612/attachments/38615/60758/HHatILC500.pdf.

[103] B. Bliewert, C. Vernieri, D. Ntounis, J. List, J. M. Torndal, and J. Tian, "Towards an update of the ILD ZHH analysis," *EPJ Web Conf.*, vol. 315, p. 01 010, 2024. arXiv: 2410.15323 [hep-ex].

[104] J. Munch Torndal, "Neutrino Correction in ZHH events," in *ILD Analysis/Software Meeting*, 2024. [Online]. Available: https://agenda.linearcollider.org/event/10545/contributions/55901/attachments/40107/63560/ILDmeeting_NuCorrection.pdf.

[105] G. Belanger *et al.*, "Full 0(alpha) electroweak corrections to double Higgs strahlung at the linear collider," *Phys. Lett. B*, vol. 576, pp. 152–164, 2003. arXiv: hep-ph/0309010.

[106] R.-Y. Zhang, W.-G. Ma, H. Chen, Y.-B. Sun, and H.-S. Hou, "Full O(alpha(ew)) electroweak corrections to e+ e- —> H H Z," *Phys. Lett. B*, vol. 578, pp. 349–358, 2004. arXiv: hep-ph/0308203.

[107] M. Cepeda *et al.*, "Report from Working Group 2: Higgs Physics at the HL-LHC and HE-LHC," *CERN Yellow Rep. Monogr.*, vol. 7, A. Dainese, M. Mangano, A. B. Meyer, A. Nisati, G. Salam, and M. A. Vesterinen, Eds., pp. 221–584, 2019. arXiv: 1902.00134 [hep-ph].

[108] J. List, B. Bliewert, D. Ntounis, J. Tian, C. Vernieri, and J. M. Torndal, "Higgs Self-coupling Strategy at Linear e+e- Colliders," *PoS*, vol. ICHEP2024, p. 079, 2025. arXiv: 2411.01507 [hep-ex].

[109] F. Arco, S. Heinemeyer, M. Mühlleitner, and K. Radchenko, "Sensitivity to triple Higgs couplings via di-Higgs production in the 2HDM at the (HL-)LHC," *Eur. Phys. J. C*, vol. 83, no. 11, p. 1019, 2023. arXiv: 2212.11242 [hep-ph].